Electronic version of an article published as:
Comput. Methods Appl. Mech. Engrg. 288, 83–109 (2015). DOI: 10.1016/j.cma.2014.11.019

Duality-Based Two-Level Error Estimation for Time-Dependent PDEs: Application to Linear and Nonlinear Parabolic Equations

G. Şimşek[†,*], X. Wu[†], K.G. van der Zee[††,*], E.H. van Brummelen[†]

[†] *Eindhoven University of Technology, Multiscale Engineering Fluid Dynamics, 5600 MB Eindhoven, Netherlands*

[††] *School of Mathematical Sciences, The University of Nottingham University Park, Nottingham NG7 2RD, United Kingdom*

Abstract

We introduce a duality-based two-level error estimator for linear and nonlinear time-dependent problems. The error measure can be a space-time norm, energy norm, final-time error or other error related functional. The general methodology is developed for an abstract nonlinear parabolic PDE and subsequently applied to linear heat and nonlinear Cahn–Hilliard equations. The error due to finite element approximations is estimated with a residual weighted approximate-dual solution which is computed with two primal approximations at nested levels. We prove that the exact error is estimated by our estimator up to higher-order remainder terms. Numerical experiments confirm the theory regarding consistency of the dual-based two-level estimator. We also present a novel space-time adaptive strategy to control errors based on the new estimator.

Contents

1 Introduction

Nonlinear time-dependent partial differential equations (PDEs) govern a large class of relevant problems in the sciences. Classical examples in mechanics include nonlinear parabolic equations such as the Navier–Stokes equations, and nonlinear hyperbolic equations such as nonlinear elastodynamics. In recent years there has been a growing interest in new nonlinear continuum-mechanics models which can be classified as phase-field models, diffuse-interface models, or generalized Cahn–Hilliard models [36]. Examples include Navier–Stokes–Cahn–Hilliard equations (multiphase flow) [25, 1], phase-field fracture [8, 7], and mechanobiological growth phenomena (e.g., tumor growth) [30, 21]. These novel models are characterized by having evolving diffuse interfaces, implicitly described by a (phase-) field variable which quickly, but smoothly, changes across an interface.

Obviously, there is a need for assessing the accuracy of numerical simulations for these problems through the use of a posteriori error estimates, and to employ these estimates to drive adaptive mesh refinement and adaptive time-step selection. Adaptivity in space is particularly useful to capture diffuse interfaces as well as other singularities. In the current work we focus on a posteriori error estimates for the semi-discrete case involving space discretizations based on Galerkin approximations, e.g., obtained using the finite element method.

*Correspondance to: G. Simsek (g.simsek@tue.nl) and K. G. van der Zee (KG.vanderZee@nottingham.ac.uk)

The subject of a posteriori error estimation for (non)linear time-dependent PDEs is classical. Its foundations (mostly studied for the parabolic case) were established in the 1990s and have been summarized in Erikkson, Estep, Hansbo, and Johnson [13]. A posteriori error estimates are typically derived in two steps: First, a measure of the error is bounded by (a dual norm of) the residual. Then, the residual is bounded by a computable quantity (usually sum of error indicators). The second step depends on the discretization at hand (see, e.g., [12] for a recent general framework).

To carry out the first step, Ref. [13] (see also [44, 29, 14]) advocate the use of the backward-in-time (linearized) dual problem. This dual problem acts as an auxiliary problem to quickly set up an exact error representation. Subsequently, invoking dual (a priori) stability bounds leads to the desired bound. Alternatively, the first step can be carried out using energy methods [28, 24], which sets up appropriate bounds on the primal (forward) problem and invokes Gronwall's inequality. Unfortunately, in both cases, the accuracy of the resulting a posteriori estimate depends on the invoked bounds (dual-based or primal-based), which is reflected by a large pre-multiplication constant (the notorious stability constant). Moreover, for *nonlinear* problems, it can be very hard to obtain quantitatively-accurate estimates because the invoked bounds typically consider worst-case scenarios, leading to huge stability constants. In this regard, we agree with Estep, Holst, and Mikulencak [16]: "[*Classical estimation*] *is generally frustrating,* [...] *we usually turn to numerical computation because analysis is too difficult. In computational error estimation, we use computation to make up for our analytical deficiencies.*". An example of the use of very intricate analytical techniques in the context of phase field models can be found in, e.g., [24, 5].

Goal-oriented a posteriori error estimates [6, 31] were developed in the late 1990s as an offspring of the above duality-based estimates for time-dependent problems as well as L^2-based estimates, and their aim is to assess the accuracy of output quantities of interest given by *functionals* of the solution. Over the years, they have been developed for time-independent, time-dependent, linear, nonlinear and coupled problems; see e.g., [22, 41, 40, 11, 39, 42]. Goal-oriented estimates are *explicit* dual-based estimates, as they directly compute an approximation to the dual problem, in contrast to the above mentioned duality techniques (where they are only used as auxiliary problems for deriving estimates). Typically, the dual approximations are computed using a richer discrete space than the primal problem (e.g., by increasing the polynomial order, or globally refining the mesh). Although goal-oriented error estimates are not necessarily (guaranteed) upper bounds (exceptions exist in the linear case [33, 34]), they are, in general, very accurate, irrespective of whether the problem is linear or nonlinear. This has motivated the current work.

In this paper, we present a novel methodology to a posteriori error estimates for non-linear time-dependent PDEs based on duality and two discretization levels. The starting point for the derivation of the estimate is the exact duality-based error representation, which is a global space–time residual weighted by the solution of the secant-linearized (backward-in-time) dual problem. The methodology for the estimate simply consists of directly evaluating this error representation with an enriched dual approximation. However, since the dual problem also depends on the exact primal solution, an additional improved *primal* approximation is computed. We thus work with two primal discretization levels and an approximate dual, and therefore call the resulting estimate a *duality-based two-level estimate*. We note that it is possible to employ the same enriched discrete space for the primal as for the dual.

Alternatively, errors can be estimated directly by using the improved primal approximation as a substitution for the exact solution. However, although it is natural for steady elliptic PDEs, this is not necessarily true for (non)linear time-dependent PDEs, as the dual problem contains the sensitivity to errors accumulated at earlier times. This information is crucial to adaptively control the accuracy of the quantity of interest.

We next wish to comment on some related works in the literature. Two-level estimators are reminiscent of, but different to, hierarchical error estimates, such as studied in [4, 43, 2, 23], where two primal discretization levels are used to define their complement (or bubble) space. In the linear elliptic case, two implicit primal levels (coarse and reconstructed) have been employed by Ovall [32, Sec. 5.2] in a duality-based estimate for seminorms, which is similar in spirit as our current work. In a goal-oriented setting, the idea of using an improved primal approximation to compute dual approximation has been discussed by Becker and Rannacher [6, Sec. 6.2], and for non-linear elasticity by Larsson, Hansbo and Runesson [27]. Also in a goal-oriented setting, two primal and dual levels have been recently employed by Perotto and Veneziani [35] and Braack, Burman and Taschenberger [9] to estimate modeling errors in hierarchical reductions and time averaging, respectively.

Following this introduction, we develop the methodology for a general (non)linear time-dependent PDE; see Section 2. We subsequently apply in Section 3 the framework to the linear heat equation and a nonlinear parabolic problem: the Cahn–Hilliard equation. Numerical results are presented in Section 4 after which we present our conclusions.

2 Duality-Based Two-Level Error Estimation

In this section, we present the general framework of the duality-based two-level error estimation. We first review the duality-based approach to a posteriori error estimates for time-dependent problems, see e.g. [6, 19, 38]. Then we present our two-level error estimate,

and prove a general consistency theorem.

2.1 Abstract time-dependent problem

We consider time-dependent semi-linear parabolic partial differential equations, for which the principal part is linear, posed in domain $\Omega \subset \mathbb{R}^d$, for a time interval $(0, T]$. A general abstract form is as follows:

Find $u : \Omega_T \to \mathbb{R}$ such that

$$\begin{aligned} \partial_t u + Bu + C(u) &= f \ \text{ in } \Omega_T := \Omega \times (0, T] \\ u(0) &= u_0 \ \text{ in } \Omega \\ \partial^*_{\mathbf{n}} u &= 0 \ \text{ on } \partial\Omega_T := \partial\Omega \times (0, T], \end{aligned} \tag{1}$$

where $\partial_t(\cdot) = \partial(\cdot)/\partial t$. We assume B to be a linear operator having a self adjoint elliptic part and C to be at least continuously Gâteaux (or Fréchet) differentiable nonlinear operator.The term $\partial^*_{\mathbf{n}}$ represents the natural boundary condition according to the application. Examples include the linear heat equation and the non-linear Cahn–Hilliard equation which will be considered in Section 3.

In order to construct weak solutions, let us introduce the function spaces $V \subset L_2(\Omega) \subset V'$. Here, V represents a suitable Sobolev space for the spatial part of the solution and V' is its dual. Hence, a suitable evolution space for u can be defined as $\mathcal{W}_{u_0} := \{v \in \mathcal{V}, \partial_t v \in \mathcal{V}' : v(0) = u_0\}$, where $\mathcal{V} := L^2(0, T; V)$ and $\mathcal{V}' := L^2(0, T; V')$ [17].

The weak form of (1) is: Find $u \in \mathcal{W}_{u_0}$:

$$\int_0^T \Big(\langle \partial_t u, v \rangle + \mathscr{B}(u, v) + \mathscr{C}(u; v) \Big)\, dt = \int_0^T \langle f, v \rangle \, dt \qquad \forall v \in \mathcal{V}, \tag{2}$$

where $\langle \omega, \nu \rangle$ is defined to be the duality pairing for any $(\omega, \nu) \in V' \times V$. Furthermore, $\mathscr{B}(\omega, \nu) := \langle B\omega, \nu \rangle$ is the bilinear form and $\mathscr{C}(\omega; \nu) := \langle C(\omega), \nu \rangle$ for all $\omega, \nu \in V$. For later use, we set $(\omega, \nu) := \int_\Omega \omega\nu \, d\Omega$ to be the L_2–inner product. Here, we use the convention that for semi-linear forms, such as $\mathscr{C}(\cdot; \cdot)$, the form is linear with respect to arguments on the right of the semicolon.

Definition 2.1 The energy norm v based on the weak formulation (2) can be introduced as

$$|\!|\!| v |\!|\!|^2_{\mathcal{W}} := \int_0^T \left(\|v_t\|^2_{V'} + \mathscr{B}^{sym}(v, v) \right) \, dt + \|v(T)\|^2, \tag{3}$$

where $\|\cdot\|_{V'} := \sup\{\langle\cdot, w\rangle : w \in V, \|w\|_V \leq 1\}$ is the dual norm and $\mathscr{B}^{sym}(\omega,\nu) = \langle B^{sym}\omega,\nu\rangle = \langle B^{sym}\nu,\omega\rangle$ for all $\omega,\nu \in V$. Here, $\mathscr{B}^{sym}$ is the self-adjoint elliptic part of $\mathscr{B}$. This is a natural norm for the abstract problem (for suitable $C(\cdot)$); see e.g. [15, Section 6.1]. □

In view of the complexity in the computation of the dual norm in (3), in this paper, we will focus on the following norm:

$$|\!|\!|v|\!|\!|^2 := \int_0^T \mathscr{B}^{sym}(v,v)\,dt + \|v(T)\|^2. \tag{4}$$

Remark 2.2 For error estimation later on, one may be alternatively interested in other norms, e.g. $|\!|\!|v|\!|\!|^2 := \int_0^T \|v\|^2_{L_2}\,dt$ or $|\!|\!|v|\!|\!|^2 := \int_0^T \|v\|^2_{H_1}\,dt$ or even output functionals, e.g. $Q(v) = \big(\bar{q}, v(T)\big)$ for a specific $\bar{q}$ (see Remark 4.2). Hence error measures of interest may differ from (4). This is possible by suitably modifying the following quantity of interest. □

Definition 2.3 (Quantity of Interest) Based on (4), the quantity of interest can be formulated as

$$Q_{q,\bar{q}}(v) = Q_q(v) + Q_{\bar{q}}(v) := \int_0^T \mathscr{B}^{sym}(q,v)\,dt + \big(\bar{q}, v(T)\big), \tag{5}$$

where $q \in \mathcal{V}$, $\bar{q} \in V$, which is essential to define the adjoint problem. Note that, $Q_{v,v(T)}(v) = |\!|\!|v|\!|\!|^2$. □

The adjoint (backward-in-time), or dual problem corresponding to (2) for $Q_{q,\bar{q}}(\cdot)$ in (5) is defined as:
Find $z_{q,\bar{q}} \in \mathcal{W}^{\bar{q}} := \{v \in \mathcal{W} : v(T) = \bar{q}\}$:

$$\int_0^T \Big(\langle -\partial_t z_{q,\bar{q}}, w\rangle + \mathscr{B}(w, z_{q,\bar{q}}) + \mathscr{C}^s(u,\hat{u}; w, z_{q,\bar{q}})\Big)\,dt = Q_q(w), \qquad \forall w \in \mathcal{V}, \tag{6}$$

where $\mathscr{C}^s(u,\hat{u}; w, z_{q,\bar{q}}) := \int_0^1 \mathscr{C}'\left(su + (1-s)\,\hat{u}; w, z_{q,\bar{q}}\right) ds$ is the mean-value linearization of the nonlinear operator, $\mathscr{C}$. Here, $\mathscr{C}'(u; w, v)$ denotes the Gâteaux (or Fréchet) derivative of $\mathscr{C}$ at u in the direction of w [6, 19, 39]:

$$\mathscr{C}'(u; w, v) = \mathscr{C}(u + w; v) - \mathscr{C}(u; v) + O(\|w\|_V^2).$$

Note that the right hand side of (6) is $Q_q(w)$, not $Q_{q,\bar{q}}(w)$ and $\bar{q}$ appears as the initial (final-time) condition for the adjoint problem in $\mathcal{W}^{\bar{q}}$.

Here, we introduced $\hat{u}$ as an arbitrary member in $\mathcal{W}_{\hat{u}_0}$ to define the linearization of the nonlinear term. In error analysis $\hat{u}$ is the approximation of u.

The strong form of the weak adjoint problem (6) can be inferred as the backward-in-time problem

$$\begin{aligned} -\partial_t z + Bz + C^s(u,\hat{u})^* z &= B^{sym} q \ \text{ in } \Omega_T \\ z(T) &= \bar{q} \ \text{ in } \Omega \\ \partial^*_{\mathbf{n}} z &= 0 \ \text{ on } \partial\Omega_T, \end{aligned} \tag{7}$$

where we denote $z_{q,\bar{q}} := z$ for simplicity. In particular, $C^s(u,\hat{u})^*$ is the adjoint of the mean value linearization of $C(u)$, such that $C^s(u,\hat{u}) := \int_0^1 C'\left(su + (1-s)\,\hat{u}\right) ds$ and

$$\mathscr{C}^s(u,\hat{u};w,z) = \langle C^s(u,\hat{u})w, z\rangle = \langle C^s(u,\hat{u})^* z, w\rangle.$$

2.2 Error representation

Let $\hat{u}$ be any approximation to the solution u, and z be the solution of the adjoint problem (7). Then we can obtain an exact representation for the error in $Q_{q,\bar{q}}(\cdot)$ in terms of adjoint-weighted residuals. Moreover, an exact error representation for the norm $|\!|\!| \cdot |\!|\!|$ follows as a corollary.

Theorem 2.A *(Error Representation) Consider an approximate solution $\hat{u} \in \mathcal{W}_{\hat{u}_0}$. Let $e := u - \hat{u}$ and $z = z_{q,\bar{q}}$ denote the dual solution in accordance with (6) for arbitrary q and $\bar{q}$. Then the error in the quantity of interest can be expressed as:*

$$Q_{q,\bar{q}}(u) - Q_{q,\bar{q}}(\hat{u}) = Q_{q,\bar{q}}(e) = \int_0^T \mathcal{R}^t\left(\hat{u};z\right) dt + \mathcal{R}^0\left(\hat{u};z\right), \tag{8}$$

where the PDE and initial-condition residuals are defined as:

$$\begin{cases} \mathcal{R}^t\left(\hat{u};z\right) := \langle f, z\rangle - \langle \partial_t \hat{u}, z\rangle - \mathscr{B}(\hat{u},z) - \mathscr{C}(\hat{u};z) \\ \mathcal{R}^0\left(\hat{u};z\right) := \left(u(0) - \hat{u}_0, z(0)\right). \end{cases} \tag{9}$$

□

Proof The proof is well-known in abstract settings, see, e.g. [6]. For the sake of completeness we provide a proof for our abstract parabolic PDE. Using the definition of the error in a quantity of interest and applying integration by parts in time to the weak dual problem (6), we get

$$\begin{aligned} Q_{q,\bar{q}}(e) &= Q_q(e) + Q_{\bar{q}}(e) \\ &= \int_0^T \Big(\langle -\partial_t z, e\rangle + \mathscr{B}(e,z) + \mathscr{C}^s(u,\hat{u};e,z) \Big)\, dt + \big(\bar{q}, e(T)\big) \\ &= \int_0^T \Big(\langle \partial_t e, z\rangle + \mathscr{B}(e,z) + \mathscr{C}^s(u,\hat{u};e,z) \Big)\, dt + \big(z(0), e(0)\big) \end{aligned} \tag{10}$$

In particular, the mean value linearization in the direction of the error, e, gives the following

$$\mathscr{C}^s(u,\hat{u};e,z) = \int_0^1 \mathscr{C}'\left(su+(1-s)\,\hat{u};e,z\right)\,ds = \mathscr{C}(u;z) - \mathscr{C}(\hat{u};z). \tag{11}$$

Then the representation of (8) can be obtained from (10) by employing (11) and the weak primal problem (2). ∎

Corollary 2.4 *(Error-in-norm Representation) Let $e = u - \hat{u}$ and choose $q = e$, $\bar{q} = e(T)$ then*

$$\|\!|e|\!\|^2 = Q_{e,e(T)}(e) = \int_0^T \mathcal{R}^t\left(\hat{u};z_{e,e(T)}\right)\,dt + \mathcal{R}^0\left(\hat{u};z_{e,e(T)}\right) \tag{12}$$

□

Proof The identities in (12) follows from a straightforward substitution in (8) using the definition (4). ∎

Remark 2.5 The choices $q = e$ and $\bar{q} = e(T)$ to get (12) lead to the adjoint problem (7) with a final-time condition driven by $e(T)$, and the PDE is driven by $B^{sym}e$. In other words, $z = z_{e,e(T)}$; it depends on e as well as u and $\hat{u}$. □

2.3 Computable Error Estimate

In Section 2.2, Theorem 2.A proves that the error in the quantity of interest can be written in terms of the residual of the approximate primal solution $\hat{u}$ and exact dual solution $z_{q,\bar{q}}$. However, it is not possible to compute the error representation (8), since the exact solution of the dual problem (7) is not available. To obtain a computable estimate, we shall employ an approximation to the dual problem. This strategy holds for (8) for any quantity of interest.

In this paper, specifically, we work with (12), where $q = e$ and $\bar{q} = e(T)$. Similar to (8), (12) is also not computable because of $z_{e,e(T)}$, which is the exact solution of (7). There are three errors involved in approximating $z_{e,e(T)}$: Linearization, primal solution approximation and dual discretization.

- Linearization error comes from $C^s(u,\hat{u})$ in (7), since it can be computed exactly only if u is available. We employ an approximation for u to approximate $C^s(u,\hat{u})$. If u is approximated with a finer mesh than $\hat{u}$, the linearization error in $C^s(u,\hat{u})$ decreases, than by simply taking $u = \hat{u}$, to get $C^s(\hat{u},\hat{u}) = C'(\hat{u})$. Therefore, we choose a finer approximation for u than $\hat{u}$.

- Primal solution approximation is required on the right-hand-side of (7). Indeed, since $q = e = u - \hat{u}$, $\bar{q} = e(T) = (u - \hat{u})(T)$ are not computable, we need a finer approximation than $\hat{u}$ for u.
- Finally, dual discretization produces an error due to dual approximation of (7).

To present the approximate dual solution and our estimate for the general framework, we will use the following notations:

- u^h = primal Galerkin approximation for coarse mesh of size h, i.e. solution of weak form (2) discretized in space replacing V by $V^h \subset V$.
- $u^{h/2}$ = primal Galerkin approximation for fine mesh of size $h/2$, i.e. solution of weak form (2) discretized in space replacing V by $V^{h/2} \supset V^h$.
- $\hat{e} := u^{h/2} - u^h$ is the difference in primal approximations.

We furthermore introduce $\hat{z}_{\hat{e},\hat{e}(T)} := \hat{z} \in \mathcal{W}^{\hat{e}(T)}$ using the following weak form

$$\int_0^T \Big(\langle -\partial_t \hat{z}, w \rangle + \mathscr{B}(w, \hat{z}) + \mathscr{C}^s(u^{h/2}, u^h; w, \hat{z}) \Big)\, dt = \int_0^T \mathscr{B}^{sym}(\hat{e}, w)\, dt, \ \forall w \in \mathcal{V}, \qquad (13)$$

which enables us to introduce that

- $\hat{z}^{h/2}_{\hat{e},\hat{e}(T)} \equiv \hat{z}^{h/2}$ (for notational convenience) is the dual approximation, i.e. solution of weak form (13) discretized in space replacing V by $V^{h/2} \supset V^h$.
- $z_{e,e(T)} = z$ (for notational convenience) is the dual solution, i.e. analytical solution of (13).

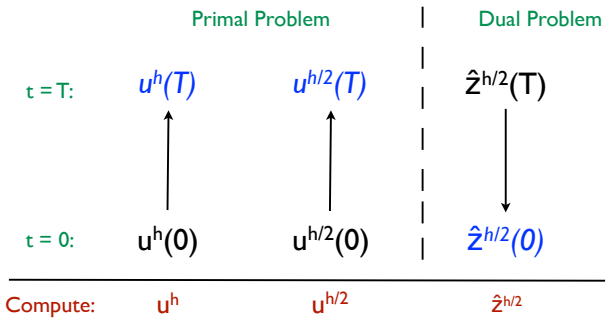

Figure 1: Required approximations in duality-based two-level error estimation

The strategy to compute $\hat{z}^{h/2}$ is illustrated in Figure 1. That is, the approximations u^h and $u^{h/2}$ are computed forward in time and subsequently $\hat{z}^{h/2}$ is obtained with a backward in time computation.

Then, we define our error estimate, Est, as:

$$Q_{e,e(T)}(u) - Q_{e,e(T)}(u^h) = \|\!|u - u^h|\!\|^2 \approx Est := \int_0^T \mathcal{R}^t\left(u^h; \hat{z}^{h/2}\right) dt + \mathcal{R}^0\left(u^h; \hat{z}^{h/2}\right) \quad (14)$$

with the residuals $\mathcal{R}^t(\cdot;\cdot)$ and $\mathcal{R}^0(\cdot;\cdot)$ defined in (9).

Note that, we simply replaced $z_{e,e(T)}$ in (12) by a computable approximation.

Remark 2.6 We approximate both the primal u and the dual z using a finer mesh than u^h. Thus, our estimate (14) is calculated with approximations on two different meshes, which motivates us to refer this procedure as *duality-based two-level* error estimation. □

The exact error is equal to the sum of the estimate in (14) and the remainder terms due to linearization, primal approximation and dual discretization errors. We shall prove that aforementioned remainders are indeed small in the following theorem:

Theorem 2.B *Let $e = u - u^h$ and $e^{h/2} := u - u^{h/2}$ for any given u^h and $u^{h/2}$. Then for the two-level secant dual solution $\hat{z}$ defined by (13), the following identity holds:*

$$\|\!|e|\!\|^2 = \int_0^T \mathcal{R}^t\left(u^h; \hat{z}\right) dt + \mathcal{R}^0\left(u^h; \hat{z}\right) + 2(\!(\!(e^{h/2}, e)\!)\!)_E - \|\!|e^{h/2}|\!\|^2. \quad (15)$$

Furthermore, for the approximation $\hat{z}^{h/2}$ of $\hat{z}$, we get the following equation:

$$\|\!|e|\!\|^2 = Est + r_1 + r_2, \quad (16)$$

with Est according to (14), and the remainders:

$$\begin{aligned} r_1 &:= 2(\!(\!(e^{h/2}, e)\!)\!)_E - \|\!|e^{h/2}|\!\|^2, \\ r_2 &:= \int_0^T \mathcal{R}^t\left(u^h; \hat{z} - \hat{z}^{h/2}\right) dt + \mathcal{R}^0\left(u^h; \hat{z} - \hat{z}^{h/2}\right), \end{aligned} \quad (17)$$

where $(\!(\!(\cdot,\cdot)\!)\!)_E$ is the inner product associated with $\|\!|\cdot|\!\|^2$. □

Remark 2.7 The remainders are such that r_1 is due to mean value linearization between $u^{h/2}$ and u^h instead of u and u^h and primal problem approximation replacing u by $u^{h/2}$; and r_2 is due to dual problem approximation. The representations in (15) and (16) appear to be the first results which combine dual-based error representations for norms with two primal discretization levels. □

Remark 2.8 The result in Theorem 2.B is dependent on $C(u)$ being Gâteaux (or Fréchet) differentiable, so that the secant form in (13). □

Remark 2.9 $\hat{z}^{h/2}$ is computed backward in time on a finer mesh using (13), than as used to compute u^h. If the dual approximation is computed on the same mesh as u^h, i.e. z^h, one would obtain a useless (unreliable) estimate from the residual computation due to Galerkin orthogonality [3]. □

Remark 2.10 If the cost of computing $u^{h/2}$ is considered excessive, higher-order reconstruction can be used to obtain a finer primal approximation; see for instance [6]. □

Proof (Proof of Theorem 2.B) Starting with (12), adding and subtracting $Q_{\hat{e},\hat{e}(T)}(\hat{e})$, and then invoking (8), gives

$$\begin{aligned}
\|\!|e|\!\|^2 = Q_{e,e(T)}(e) &= \int_0^T \mathcal{R}^t\left(u^h; z\right)\, dt + \mathcal{R}^0\left(u^h; z\right) + Q_{\hat{e},\hat{e}(T)}(\hat{e}) - Q_{\hat{e},\hat{e}(T)}(\hat{e}) \\
&= \int_0^T \mathcal{R}^t\left(u^h; z\right)\, dt + \mathcal{R}^0\left(u^h; z\right) \\
&+ \int_0^T \mathcal{R}^t\left(u^h; \hat{z}\right)\, dt + \mathcal{R}^0\left(u^h; \hat{z}\right) - \int_0^T \mathcal{R}^t\left(u^h; \hat{z}\right)\, dt - \mathcal{R}^0\left(u^h; \hat{z}\right)
\end{aligned}$$

Then due to semi-linear property of $\mathcal{R}^t(\cdot;\cdot)$ and $\mathcal{R}^0(\cdot;\cdot)$, we get

$$\|\!|e|\!\|^2 = Q_{e,e(T)}(e) = \int_0^T \mathcal{R}^t\left(u^h; \hat{z}\right)\, dt + \mathcal{R}^0\left(u^h; \hat{z}\right) + \int_0^T \mathcal{R}^t\left(u^h; z - \hat{z}\right)\, dt + \mathcal{R}^0\left(u^h; z - \hat{z}\right).$$

Following from the equation above, we employ (12) again for e and $\hat{e}$:

$$\|\!|e|\!\|^2 = \int_0^T \mathcal{R}^t\left(u^h; \hat{z}\right)\, dt + \mathcal{R}^0\left(u^h; \hat{z}\right) + Q_{e,e(T)}(e) - Q_{\hat{e},\hat{e}(T)}(\hat{e}) \tag{18}$$

The last two terms of (18) can be extended in terms of inner products:

$$Q_{e,e(T)}(e) - Q_{\hat{e},\hat{e}(T)}(\hat{e}) = \|\!|e|\!\|^2 - \|\!|\hat{e}|\!\|^2 = (\!(\!(e - \hat{e}, e + \hat{e})\!)\!)_E. \tag{19}$$

Next, writing $e, e^{h/2}$ and $\hat{e}$ in (19) in terms of u, u^h and $u^{h/2}$, adding and subtracting u in the inner product and using linearity of inner product gives

$$\begin{aligned}
Q_{e,e(T)}(e) - Q_{\hat{e},\hat{e}(T)}(\hat{e}) &= (\!(\!(u - u^{h/2}, u - 2u^h + u^{h/2} + u - u)\!)\!)_E \\
&= (\!(\!(e^{h/2}, 2e - e^{h/2})\!)\!)_E \\
&= 2(\!(\!(e^{h/2}, e)\!)\!)_E - \|\!|e^{h/2}|\!\|^2,
\end{aligned} \tag{20}$$

which proves (15).

We need the approximate dual $\hat{z}^{h/2}$ to obtain (16). By adding and subtracting the terms $\int_0^T \mathcal{R}^t\left(u^h;\hat{z}^{h/2}\right)\,dt$ and $\mathcal{R}^0\left(u^h;\hat{z}^{h/2}\right)$ to (15), we get:

$$\begin{aligned}
|\!|\!|e|\!|\!|^2 &= \int_0^T \mathcal{R}^t\left(u^h;\hat{z}^{h/2}\right)\,dt + \mathcal{R}^0\left(u^h;\hat{z}^{h/2}\right) + 2(\!(\!(e^{h/2},e)\!)\!)_E - |\!|\!|e^{h/2}|\!|\!|^2 \\
&\quad + \int_0^T \mathcal{R}^t\left(u^h;\hat{z}-\hat{z}^{h/2}\right)\,dt + \mathcal{R}^0\left(u^h;\hat{z}-\hat{z}^{h/2}\right) \\
&= Est + 2(\!(\!(e^{h/2},e)\!)\!)_E - |\!|\!|e^{h/2}|\!|\!|^2 + \int_0^T \mathcal{R}^t\left(u^h;\hat{z}-\hat{z}^{h/2}\right)\,dt + \mathcal{R}^0\left(u^h;\hat{z}-\hat{z}^{h/2}\right). \quad \blacksquare
\end{aligned}$$

3 Applications

In this section, we will consider heat and Cahn–Hilliard equations representative of a linear and nonlinear application, respectively.

3.1 Heat Equation

We choose $Bu = -\triangle u$, where $B^{sym}u = Bu$ and $C(u) = 0$ in the general abstract form (1) and obtain the following heat equation:

$$\begin{aligned}
\partial_t u - \triangle u &= f \ \text{ in } \Omega_T \\
u(0) &= u_0 \ \text{ in } \Omega \\
u &= 0 \ \text{ on } \partial\Omega_T,
\end{aligned} \tag{21}$$

The weak form of (21) is defined by substituting the self-adjoint linear and nonlinear terms, Bu and $C(u)$, respectively in (2) and by choosing the function spaces as $V = H^1(\Omega)$, $V' = H^{-1}(\Omega)$, so $\mathcal{V} := L^2\left(0,T;H^1(\Omega)\right)$, $\mathcal{V}' := L^2\left(0,T;H^{-1}(\Omega)\right)$.

Using (4) with $\mathscr{B}^{sym}(u,v) = \int_\Omega \nabla u\cdot\nabla v$, we have the energy norm:

$$|\!|\!|u|\!|\!|_E^2 = \int_0^T \|\nabla u\|^2\,dt + \|u(T)\|^2.$$

The semi-discrete primal problem can be written as: [1]

[1]For conciseness, we present the weak formulations in Section 3 in their equivalent time–dependent form, without integration in time.

Find $u^h(t) \in V^h$:

$$\begin{aligned} \langle \partial_t u^h, v\rangle + (\nabla u^h, \nabla v) &= \langle f, v\rangle, \ \forall v \in V^h, \text{a.e. } t \\ u^h(0) &= \pi_{V^h} u_0 \end{aligned} \tag{22}$$

Here, V^h is a discrete subset of V consisting of e.g. continuous finite element functions on a predefined mesh and π_{V^h} is the L_2-projection of u_0 onto V^h.

Following (6) and (13), the weak dual form gives:

Find $z \in \mathcal{W}^{e(T)}$:

$$\begin{aligned} -\langle \partial_t z, w\rangle + (\nabla z, \nabla w) &= (\nabla e, \nabla w), \ \ \forall w \in V, \text{a.e. } t \\ z(T) &= e(T), \end{aligned} \tag{23}$$

where $e = u - u^h$ with $\bar{q} = e(T)$, $q = e$. In (23), all of the terms on the left hand side are independent of u, u^h, since the heat equation is linear. Thus $z_{e,e(T)} = \hat{z}_{\hat{e},\hat{e}(T)}$ in the case that u is replaced by $u^{h/2}$ on the right-hand-side.

Corollary 3.1 *For approximations to the heat equation (21), the error satisfies the representation (15) in Theorem 2.B, with $\hat{z}$, the solution of (23) where u is replaced by $u^{h/2}$. Next let the approximation $\hat{z}^{h/2} \in V^{h/2}$ be defined by:*

$$\langle -\partial_t \hat{z}^{h/2}, w\rangle + (\nabla \hat{z}^{h/2}, \nabla w) = \left(\nabla \left(u^{h/2} - u^h\right), \nabla w\right), \ \forall w \in V^{h/2}, \text{a.e. } t \tag{24}$$

with initial condition $\hat{z}^{h/2}(T) = \left(u^{h/2} - u^h\right)(T)$.

Then, the computable estimate reduces to

$$Est = \int_0^T \mathcal{R}^t\left(u^h; \hat{z}^{h/2}\right) dt + \mathcal{R}^0\left(u^h; \hat{z}^{h/2}\right) \tag{25}$$

with (21):

$$\begin{aligned} \mathcal{R}^t\left(u^h; \hat{z}^{h/2}\right) &= \langle f, \hat{z}^{h/2}\rangle - (\nabla u^h, \nabla \hat{z}^{h/2}) - \langle \partial_t u^h, \hat{z}^{h/2}\rangle \\ \mathcal{R}^0\left(u^h; \hat{z}^{h/2}\right) &= \left(u_0^{h/2} - u_0^h; \hat{z}^{h/2}(0)\right) \end{aligned} \tag{26}$$

for which it holds that

$$|\!|\!| e |\!|\!|^2 = Est + r_1 + r_2. \tag{27}$$

In particular, r_1 and r_2 are given explicitly in Theorem 2.B. □

Proof The error satisfies (15) by the first part of the proof of Theorem 2.B for which we use the approximation u^h and the solution $\hat{z}$ for the heat equation. (25) is introduced in the same form as (14) and the identities in (26) are obtained following (9) in Theorem 2.A using the primal approximation u^h in (22) instead of $\hat{u}$ and the dual approximation $\hat{z}^{h/2}$ defined in (24) instead of z. Then (27) is a straightforward result following from Theorem 2.B. ■

3.2 The Convective Cahn–Hilliard Equation

Next we consider the convective Cahn–Hilliard equation, in a convex domain Ω by choosing $Bu = \nabla \cdot (\mathbf{v}u) + \frac{\varepsilon^2}{Pe}\triangle(\triangle u)$, with $B^{sym} = \frac{\varepsilon^2}{Pe}\triangle(\triangle u)$ and $C(u) = -\frac{1}{Pe}\triangle\phi'(u)$, where $\mathbf{v}$ is a given smooth velocity field, satisfying $\operatorname{div}\mathbf{v} = 0$, Pe is the *Péclet* number and ε is the interface thickness parameter. $\phi(u)$ is the nonlinear (bulk) free-energy density function, which is a C^2-continuous, double well potential function. A common choice which we adopt is:

$$\phi(u) := \frac{1}{4}\left(u^2 - 1\right)^2.$$

The equation then becomes

$$\begin{aligned} \partial_t u + \nabla \cdot (\mathbf{v}u) + \frac{1}{Pe}\triangle\left(\varepsilon^2\triangle u - \phi'(u)\right) = 0 \ \text{ in } \Omega_T \\ u(0) = u_0 \ \text{ in } \Omega \\ \partial_{\mathbf{n}} u = 0 \ \text{ on } \partial\Omega_T \\ \partial_{\mathbf{n}}\left(\varepsilon^2\triangle u - \phi'(u)\right) = 0 \ \text{ on } \partial\Omega_T \end{aligned} \tag{28}$$

The choices Bu and $C(u)$ lead to a fourth-order nonlinear parabolic equation, for which we define the function spaces as $\mathcal{V} := L^2(0,T;H^2(\Omega))$ and $\mathcal{V}' := L^2(0,T;H^2(\Omega)')$, with $V = H^2(\Omega)$ and $V' = H^2(\Omega)'$.

The corresponding energy norm from (4) with $\mathscr{B}^{sym}(u,v) = \int_\Omega \frac{\varepsilon^2}{Pe}\triangle u \cdot \triangle v$:

$$|\!|\!| u |\!|\!|_E^2 := \int_0^T \frac{\varepsilon^2}{Pe}\|\triangle u\|^2\, dt + \|u(T)\|^2$$

The semi-discrete problem can be defined as:

Find $u^h(t) \in V^h$:

$$\begin{aligned} \langle \partial_t u^h, v\rangle + (\mathbf{v}\nabla u^h, v) + \frac{1}{Pe}\Big(\varepsilon^2\left(\triangle u^h, \triangle v\right) + (\nabla\phi'(u^h), \nabla v)\Big) = 0, \ \ \forall v \in V^h, \text{ a.e.} t \\ u^h(0) = \pi_{V^h} u_0, \end{aligned} \tag{29}$$

where $\pi_{V^h}u_0$ an L_2-projection of u_0 onto discrete space V^h. Here, $V = H^2(\Omega)$ and V^h is a subset of V consisting of, e.g. two times differentiable shape functions.

Then employing (6) with $\mathscr{C}^s(u,u^h;w,z) = \int_\Omega \frac{1}{Pe}\triangle\phi'^s(u,u^h)wz\, d\Omega$ gives the weak dual of (28) as:

Find $z \in \mathcal{W}^{e(T)}$:

$$\langle -\partial_t z, w\rangle - (\mathbf{v}\nabla z, w) + \frac{1}{Pe}\Big(\left(\varepsilon^2\triangle z, \triangle w\right) + \left(\nabla\phi'^s(u,u^h)z, \nabla w\right)\Big) = \left(-\frac{\varepsilon^2}{Pe}\triangle e, \triangle w\right), \tag{30}$$

for all $w \in V$ almost every t with "initial"' condition $z(T) = e(T)$, where $\mathcal{W}^{e^u(T)} = \left\{v \in \mathcal{V}, \partial_t v \in \mathcal{V}' := L^2(0,T;H^{-1}(\Omega)) : v(T) = u(T) - u^h(T)\right\}$.

$\phi'^s(u,u^h)$ is the mean-value linearization of $\phi'(u)$ such that:

$$\phi'^s(u,u^h) = \int_0^1 \phi''\left(su + (1-s)\,u^h\right)\,ds = u^2 + (u^h)^2 + uu^h - 1.$$

The right hand side of (30) shows that the dual problem is driven by $e = u - u^h$, while the left hand side shows the dependence on u, u^h due to the nonlinear term.

Corollary 3.2 *The error in the energy-norm for the convective Cahn–Hilliard equation satisfies (15) in Theorem 2.B with u^h, solution of (29) and $\hat{z}$, solution of (30) for u is replaced by $u^{h/2}$. Let also the approximation $\hat{z}^{h/2}(t) \in V^{h/2}$ be defined by:*

$$\begin{aligned}\langle -\partial_t \hat{z}^{h/2}, w\rangle - \left(\mathbf{v}\nabla\hat{z}^{h/2}, w\right) + \frac{1}{Pe}\Big(\left(\varepsilon^2\triangle\hat{z}^{h/2}, \triangle w\right) + \left(\nabla\phi'^s(u^{h/2},u^h)\hat{z}^{h/2}, \nabla w\right)\Big) \\ = \left(-\frac{\varepsilon^2}{Pe}\triangle(u^{h/2}-u^h), \triangle w\right),\end{aligned} \tag{31}$$

$\forall w \in V^{h/2}$ *almost every t, with "initial" condition* $\hat{z}^{h/2}(T) = \left(u^{h/2} - u^h\right)(T)$.

The computable estimate then becomes

$$Est = \int_0^T \mathcal{R}^t\left(u^h; \hat{z}^{h/2}\right)\,dt + \mathcal{R}^0\left(u^h; \hat{z}^{h/2}\right) \tag{32}$$

where

$$\begin{aligned}\mathcal{R}^t\left(u^h; \hat{z}^{h/2}\right) &= -\langle\partial_t u^h, \hat{z}^{h/2}\rangle - (\mathbf{v}\nabla u^h, \hat{z}^{h/2}) - \frac{1}{Pe}\Big(\varepsilon^2(\triangle u^h, \triangle\hat{z}^{h/2}) - (\nabla\phi'(u^h), \nabla\hat{z}^{h/2})\Big) \\ \mathcal{R}^0\left(u^h; \hat{z}^{h/2}\right) &= \left(u_0^{h/2} - u_0^h(0), \hat{z}^{h/2}(0)\right),\end{aligned} \tag{33}$$

for which it holds that:

$$\left|\!\left|\!\left|e\right|\!\right|\!\right|^2 = Est + r_1 + r_2 \tag{34}$$

with r_1 and r_2 introduced in Theorem 2.B. □

Proof The error satisfies (15) by employing the first part of the proof in Theorem 2.B with u^h and $\hat{z}$ of Cahn–Hilliard equation. The computable estimate (32) is in the same form as (14), for which the residuals in (33) are computed using approximation u^h in (29) and approximation $\hat{z}^{h/2}$ in (31). Then (34) is straightforward result of Theorem 2.B. ■

Computing the approximate solutions u^h, $u^{h/2}$ and $z^{h/2}$ need higher-order discrete spaces with C^1-continuity. These have been pursued in [20] and [37]. In order to avoid the direct spatial discretization of a fourth-order operator in numerical computations, we continue in the next section with the Cahn–Hilliard equation in a mixed formulation as two second-order equations.

3.2.1 Mixed Formulation of the Convective Cahn–Hilliard Equation

In the mixed formulation, a new variable μ, called chemical potential is introduced. The the set of equations becomes

$$\begin{aligned} \partial_t u + \nabla \cdot (\mathbf{v}u) - \frac{1}{Pe}\triangle\mu = 0 \ \text{ in } \Omega_T \\ \mu - \phi'(u) + \varepsilon^2 \triangle u = 0 \ \text{ in } \Omega_T \\ u(0) = u_0 \ \text{ in } \Omega \\ \partial_{\mathbf{n}} u = \partial_{\mathbf{n}} \mu = 0 \ \text{ on } \partial\Omega_T. \end{aligned} \tag{35}$$

System (35) does not immediately fit the general form in (2). Nevertheless, the general setting can be straightforwardly extended to account for systems.

We will set the corresponding energy norm as:

$$|\!|\!| (u,\mu) |\!|\!|_E^2 := \int_0^T \left(\varepsilon^2 \|\nabla u\|^2 + \frac{1}{Pe}\|\nabla\mu\|^2 \right) dt + \|u(T)\|^2. \tag{36}$$

The weak form of (35) becomes:

Find $(u,\mu) \in \mathcal{W}_{u_0} \times \mathcal{V}$

$$\begin{aligned} \langle u_t, v\rangle + (\mathbf{v}\nabla u, v) + \frac{1}{Pe}(\nabla\mu, \nabla v) = 0, \ \ \forall v \in V \\ (\mu, w) - (\phi'(u), w) - \varepsilon^2 (\nabla u, \nabla w) = 0, \ \ \forall w \in V, \end{aligned} \tag{37}$$

where $\mathcal{V} = L^2(0,T;H^1(\Omega))$ and $\mathcal{W}_{u_0} = \{v \in \mathcal{V}, \partial_t v \in \mathcal{V}' := L^2(0,T;H^{-1}(\Omega)) : v(0) = u_0\}$
The semi-discrete weak form of (35) is:

Find $u^h(t), \mu^h(t) \in V^h$

$$\begin{aligned} \langle \partial_t u^h, v\rangle + \left(\mathbf{v}\nabla u^h, v\right) + \frac{1}{Pe}\left(\nabla\mu^h, \nabla v\right) = 0, \ \ \forall v \in V^h \\ \left(\mu^h, w\right) - \left(\phi'(u^h), w\right) - \varepsilon^2 \left(\nabla u^h, \nabla w\right) = 0, \ \ \forall w \in V^h \\ u^h(0) = \pi_{V^h} u_0, \end{aligned} \tag{38}$$

for almost every t and $V^h \subset V = H^1(\Omega)$.

The weak dual system of mixed formulation is (see [39]):
Find $(z,\chi) \in \mathcal{W}^{e^u(T)} \times \mathcal{V}$:

$$\begin{aligned} \langle -\partial_t z, \nu\rangle - (\mathbf{v}\nabla z, \nu) - \varepsilon^2 (\nabla\chi, \nabla\nu) - \left(\phi'^s(u,u^h)\chi, \nu\right) &= \varepsilon^2 (\nabla e^u, \nabla\nu) \\ (\chi,\eta) + \frac{1}{Pe}(\nabla z, \nabla\eta) &= \frac{1}{Pe}(\nabla e^\mu, \nabla\eta) \\ z(T) &= e^u(T) \end{aligned} \tag{39}$$

for almost every t and for all $\nu, \eta \in V$, where (z,χ) is the dual pair of (u,μ) and $\phi'^s(u,u^h)$ is the mean-value linearization of $\phi'(u)$ as in Section 3.2.

The right hand side of (39) shows that the dual problem is driven by the approximation error in u and μ, which are $e^u := u - u^h$ and $e^\mu := \mu - \mu^h$, while the term $\phi'^s(u,u^h)$ on the left hand side is dependent on u and u^h due to linearization. Furthermore, the dual space for z can be defined as $\mathcal{W}^{e^u(T)} = \left\{v \in \mathcal{V}, \partial_t v \in \mathcal{V}' := L^2(0,T;H^{-1}(\Omega)) : v(T) = e^{u(T)} = u(T) - u^h(T)\right\}$

Proposition 3.3 *Let $(\hat{z},\hat{\chi})$ be the solution pair of (39) for u and μ are replaced by $u^{h/2}$ and $\mu^{h/2}$, respectively. Then the error measure for mixed formulation of Cahn–Hilliard equation satisfies:*

$$\begin{aligned} |\!|\!| (e^u, e^\mu) |\!|\!|^2 = \int_0^T \left(\mathcal{R}_1^t\left(u^h;\hat{z}\right) + \mathcal{R}_2^t\left(\mu^h;\hat{\chi}\right)\right) dt + \mathcal{R}^0\left(u^h;\hat{z}\right) \\ + 2(\!(\!((e^{u^{h/2}}, e^{\mu^{h/2}}), (e^u, e^\mu))\!)\!)_E - |\!|\!|(e^{u^{h/2}}, e^{\mu^{h/2}})|\!|\!|^2, \end{aligned} \tag{40}$$

where $e^u = u - u^h$, $e^\mu = \mu - \mu^h$ and $e^{u^{h/2}} = u - u^{h/2}$, $e^{\mu^{h/2}} = \mu - \mu^{h/2}$ for any given $u^h, u^{h/2}, \mu^h$ and $\mu^{h/2}$.

Furthermore, for $\left(\hat{z}^{h/2}, \hat{\chi}^{h/2}\right)$ of $(\hat{z},\hat{\chi})$, we get:

$$|\!|\!| (e^u, e^\mu) |\!|\!|^2 = Est + r_1 + r_2, \tag{41}$$

where

$$Est = \int_0^T \left(\mathcal{R}_1^t\left(u^h;\hat{z}^{h/2}\right) + \mathcal{R}_2^t\left(\mu^h;\hat{\chi}^{h/2}\right)\right) dt + \mathcal{R}^0\left(u^h;\hat{z}^{h/2}\right) \tag{42}$$

with residuals

$$\begin{aligned} \mathcal{R}_1^t\left(u^h;\hat{z}^{h/2}\right) &= -\langle\partial_t u^h, \hat{z}^{h/2}\rangle - (\mathbf{v}\nabla u^h, \hat{z}^{h/2}) - \frac{1}{Pe}(\nabla\mu^h, \nabla\hat{z}^{h/2}) \\ \mathcal{R}_2^t\left(\mu^h;\hat{\chi}^{h/2}\right) &= -(\mu^h, \hat{\chi}^{h/2}) + (\phi'(u^h), \hat{\chi}^{h/2}) + \varepsilon^2(\nabla u^h, \nabla\hat{\chi}^{h/2}) \\ \mathcal{R}^0\left(u^h;\hat{z}^{h/2}\right) &= \left(u_0^{h/2} - u_0^h, \hat{z}^{h/2}(0)\right). \end{aligned} \tag{43}$$

and the remainders

$$
\begin{aligned}
r_1 &:= 2(\!(\!((e^{u^{h/2}}, e^{\mu^{h/2}}), (e^u, e^\mu))\!)\!)_E - \|\!|(e^{u^{h/2}}, e^{\mu^{h/2}})|\!\|^2, \\
r_2 &:= \int_0^T \left(\mathcal{R}_1^t \left(u^h; \hat{z} - \hat{z}^{h/2}\right) + \mathcal{R}_2^t \left(\mu^h; \hat{\chi} - \hat{\chi}^{h/2}\right) \right) dt + \mathcal{R}^0 \left(u^h; \hat{z} - \hat{z}^{h/2}\right).
\end{aligned} \tag{44}
$$

□

Proof We can not apply Theorem 2.B, but we closely follow its proof. Using (36), the error writes:

$$
\begin{aligned}
\|\!| (e^u, e^\mu) |\!\|^2 = Q_{e^u, e^\mu, e^u(T)} (e^u, e^\mu) &= \int_0^T \left(\frac{\varepsilon^2}{Pe} \|\nabla e^u\|^2 + \frac{1}{Pe} \|\nabla e^\mu\|^2 \right) dt + \|u(T)\|^2 \\
&= \int_0^T \left(\mathcal{R}_1^t \left(u^h; z\right) + \mathcal{R}_2^t \left(\mu^h; \chi\right) \right) dt + \mathcal{R}^0 \left(u^h; z\right)
\end{aligned}
$$

Then by adding and subtracting $Q_{\hat{e}^u, \hat{e}^\mu, \hat{e}^u(T)} (\hat{e}^u, \hat{e}^\mu)$ with $\hat{e}^u := u^{h/2} - u^h$ and $\hat{e}^\mu := \mu^{h/2} - \mu^h$ and due to semi-linearity of $\mathcal{R}$, the error representation becomes:

$$
\begin{aligned}
\|\!| (e^u, e^\mu) |\!\|^2 &= \int_0^T \left(\mathcal{R}_1^t \left(u^h; z\right) + \mathcal{R}_2^t \left(\mu^h; \chi\right) \right) dt + \mathcal{R}^0 \left(u^h; z\right) + Q_{\hat{e}^u, \hat{e}^\mu, \hat{e}^u(T)} (\hat{e}^u, \hat{e}^\mu) \\
&- Q_{\hat{e}^u, \hat{e}^\mu, \hat{e}^u(T)} (\hat{e}^u, \hat{e}^\mu) \\
&= \int_0^T \left(\mathcal{R}_1^t \left(u^h; \hat{z}\right) + \mathcal{R}_2^t \left(\mu^h; \hat{\chi}\right) \right) dt + \mathcal{R}^0 \left(u^h; \hat{z}\right) \\
&+ \int_0^T \left(\mathcal{R}_1^t \left(u^h; z - \hat{z}\right) + \mathcal{R}_2^t \left(\mu^h; \chi - \hat{\chi}\right) \right) dt + \mathcal{R}^0 \left(u^h; z - \hat{z}\right) \\
&= \int_0^T \left(\mathcal{R}_1^t \left(u^h; \hat{z}\right) + \mathcal{R}_2^t \left(\mu^h; \hat{\chi}\right) \right) dt + \mathcal{R}^0 \left(u^h; \hat{z}\right) + Q_{e^u, e^\mu, e^u(T)} (e^u, e^\mu) \\
&- Q_{\hat{e}^u, \hat{e}^\mu, \hat{e}^u(T)} (\hat{e}^u, \hat{e}^\mu)
\end{aligned} \tag{45}
$$

We can extend the last two terms in (45) in terms of inner products and write the errors in terms of $u, u^h, u^{h/2}$ and $\mu, \mu^h, \mu^{h/2}$.

$$
Q_{e^u, e^\mu, e^u(T)} (e^u, e^\mu) - Q_{\hat{e}^u, \hat{e}^\mu, \hat{e}^u(T)} (\hat{e}^u, \hat{e}^\mu) = \|\!| (e^u, e^\mu) |\!\|^2 - \|\!| (\hat{e}^u, \hat{e}^\mu) |\!\|^2
$$

Then using linearity of the inner product after adding and subtracting u and μ to the second part of the product gives

$$
\begin{aligned}
\|\!| (e^u, e^\mu) |\!\|^2 - \|\!| \left(e^{\hat{u}}, e^{\hat{\mu}}\right) |\!\|^2 &= (\!(\!((e^u, e^\mu) - (\hat{e}^u, \hat{e}^\mu), (e^u, e^\mu) + (\hat{e}^u, \hat{e}^\mu))\!)\!)_E \\
&= (\!(\!(u - u^{h/2} + \mu - \mu^{h/2}, u - 2u^h + \mu - 2\mu^h + u^{h/2} + \mu^{h/2} \\
&\qquad + u - u + \mu - \mu)\!)\!)_E \\
&= (\!(\!((e^{u^{h/2}}, e^{\mu^{h/2}}), 2(e^u, e^\mu) - (e^{u^{h/2}}, e^{\mu^{h/2}}))\!)\!)_E \\
&= 2(\!(\!((e^{u^{h/2}}, e^{\mu^{h/2}}), (e^u, e^\mu))\!)\!)_E - \|\!|(e^{u^{h/2}}, e^{\mu^{h/2}})|\!\|^2
\end{aligned}
$$

which proves (40).

Next, if we add and subtract the terms $\int_0^T \left(\mathcal{R}_1^t \left(u^h; \hat{z}^{h/2} \right) + \mathcal{R}_2^t \left(\mu^h; \hat{\chi}^{h/2} \right) \right) dt + \mathcal{R}^0 \left(u^h; \hat{z}^{h/2} \right)$ from (40), we obtain (41) such that

$$
\begin{aligned}
\| \! | \left(e^u, e^\mu \right) | \! \|^2 = & \int_0^T \left(\mathcal{R}_1^t \left(u^h; \hat{z}^{h/2} \right) + \mathcal{R}_2^t \left(\mu^h; \hat{\chi}^{h/2} \right) \right) dt + \mathcal{R}^0 \left(u^h; \hat{z}^{h/2} \right) \\
& + 2 (\!(\!(\left(e^{u^{h/2}}, e^{\mu^{h/2}} \right), \left(e^u, e^\mu \right))\!)\!)_E - \| \! | \left(e^{u^{h/2}}, e^{\mu^{h/2}} \right) | \! \|^2 \\
& + \int_0^T \left(\mathcal{R}_1^t \left(u^h; \hat{z} - \hat{z}^{h/2} \right) + \mathcal{R}_2^t \left(\mu^h; \hat{\chi} - \hat{\chi}^{h/2} \right) \right) dt + \mathcal{R}^0 \left(u^h; \hat{z} - \hat{z}^{h/2} \right),
\end{aligned}
$$

which gives the computable estimate (42). In particular, one can obtain the residuals (43) following the proof of Theorem 2.A. ∎

4 Numerics

In this section, the performance of the duality-based two-level estimator is illustrated for linear heat and nonlinear convective Cahn–Hilliard equations. We focus on errors due to spatial discretization.

For discretization in space, we use piecewise linear finite element approximations for the heat equation and the mixed formulation of the Cahn–Hilliard equation. For time discretization, we use the backward Euler method for the heat equation and a first-order semi-implicit splitting scheme from [18] for Cahn–Hilliard equation. Recent second-order time schemes for Cahn–Hilliard models can be found in [46, 47]. In the numerical experiments, the time step is chosen sufficiently small for both of the equations, in order to avoid time errors due to time discretization.

The results will be investigated in two parts: The first part, Section 4.1, is about the convergence of the estimate (14) under uniform space refinements. The second part, Section 4.2, is devoted to adaptivity. In this section we consider adaptive mesh-refinement employing the duality-based two-level error estimates.

Remark 4.1 The general estimate Est introduced in (14) is localized in this section both in space and in time. In particular, the results presented in Section 4.1, computes Est by localizing only in time, but global in space. However, in Section 4.2, the indicator is obtained by localizing Est both in time and space. □

4.1 Convergence and Effectivity

We test the convergence against true errors and present effectivity indices for 1D and 2D test cases. Effectivity is the ratio of the estimator to the true error:

$$\text{Effectivity} = \frac{Est}{Q_{e,e(T)}(e)} = \frac{Est}{\|\!|e|\!\|^2}.$$

Effectivity values in the range $0.1 \sim 10$ are generally considered acceptable, however, ideally it is close to 1.

4.1.1 Heat Equation

We first consider the linear heat equation with zero Dirichlet boundary conditions. We computed heat equation for single and 100 time steps in $\Omega = [0,1]^d$ with $d \in \{1,2\}$. Here, heat equation is considered in the case of absence of source, that is, $f = 0$.

To evaluate the estimate Est, space-time approximations are required. The backward Euler scheme yields approximations u_k^h, at discrete time instances. We define all approximations u^h, $u^{h/2}$ and $\hat{z}^{h/2}$ using a piecewise-constant reconstruction for all $t \in [0,T]$ such that

$$u^h(t) = u_{k+1}^h, \quad t \in \big(t_k, t_{k+1}\big]$$
$$\hat{z}^{h/2}(t) = \hat{z}_{k+1}^{h/2}, \quad t \in \big[t_k, t_{k+1}\big)$$

for $k = 0, \ldots, N-1$, then (25) becomes[2]

$$Est = \sum_{k=0}^{N-1} \Big\{ \Delta t \Big(\langle f_{k+1}, \hat{z}_k^{h/2} \rangle - (\nabla u_{k+1}^h, \nabla \hat{z}_k^{h/2}) \Big) - (u_{k+1}^h - u_k^h, \hat{z}_k^{h/2}) \Big\}. \tag{46}$$

We can compute part of the estimate at each time step and sum up to the final time, T.

1D Simulation We take the initial data as:

$$u(x,0) = \sin(\pi x),\ x \in [0,1]$$

[2]One can not immediately substitute piecewise-constant reconstruction in the representation formula (25) because of u_t. To obtain the result (46), one can use a limiting procedure on a continuous piecewise linear function. For example, use the following reconstruction

$$u^h(t) = \begin{cases} \frac{u_{k+1}-u_k}{t_{k+\epsilon}-t_k}(t - t_{k+\epsilon}) + u_{k+1} & \text{for } t_k < t \le t_{k+\epsilon}; \\ u_{k+1} & \text{for } t_{k+\epsilon} < t \le t_{k+1}. \end{cases}$$

which is defined for $t \in (t_k, t_{k+1}]$ to compute the stepwise time integration and take the limit of $\epsilon \to 0$.

and compute $u^h \in V^h$ with $2^3, 2^4, \ldots, 2^9$ elements, i.e. $h = 2^{-3}, 2^{-4}, \ldots, 2^{-9}$. We use time step size $\Delta t = 0.0005$. The overkill solution for the exact error is computed using 2^{13} elements. To compute the dual, we use a uniformly refined space $V^{h/2}$ with $2^4, \ldots, 2^{10}$ elements. We also investigate the use of a better, but two times more expensive space $V^{h/4}$ instead of $V^{h/2}$ with $2^5, \ldots, 2^{11}$ elements.

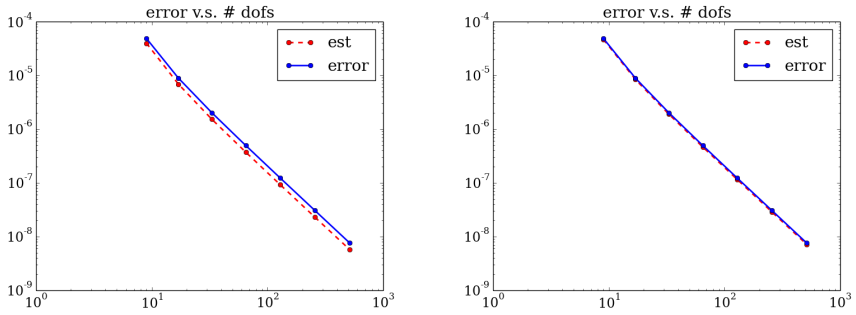

Figure 2: Convergence of error and estimate Est with respect to uniform refinement for single time step with two levels V^h and $V^{h/2}$ (left),and V^h and $V^{h/4}$ (right) for heat equation in 1D.

We choose $q = u - u^h$ and $\bar{q} = u(T) - u^h(T)$ as in (23) and to compute the dual approximation, u is replaced with the approximations in $V^{h/2}$ and $V^{h/4}$. In Figure 2, we see that the estimate asymptotically bounds the error up to a constant which confirms the effectivity of the two-level estimate.

Nb of Elems	Eff $(u^h; \hat{z}^{h/2})$	Eff $(u^h; \hat{z}^{h/4})$
16	0.77210875	0.94439973
32	0.75602279	0.93939171
64	0.75158218	0.93803695
128	0.75056921	0.93784922
256	0.75082958	0.93844620

Table 1: Effectivity of single time step estimate for heat equation in 1D.

In Table 1, the effectivity indices are displayed for the dual approximations computed in the two different discrete spaces (i.e. $V^{h/2}$ and $V^{h/4}$). The accuracy of the estimate increases when $\hat{z}^{h/4}$ is used instead of $\hat{z}^{h/2}$ to compute Est.

We also tested the effectivity of (46) for $T = 0.05$ with 100 time steps in Figure 3. The estimate asymptotically follows the error up to a constant which gives the effectivity index. Accordingly, Table 2 presents the error, estimates and the effectivity for dual approximation

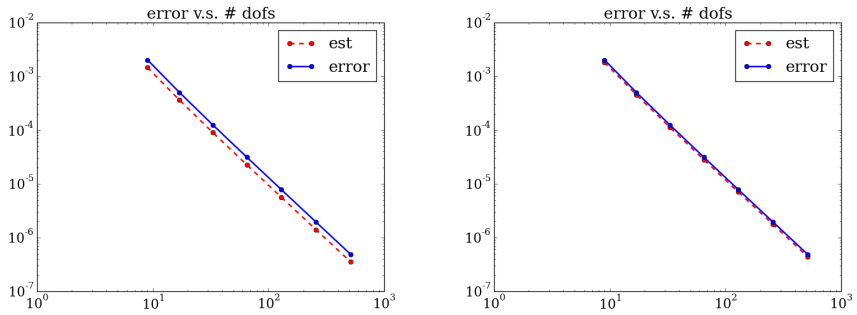

Figure 3: Convergence of error and estimate Est with respect to uniform refinement for 100 time steps with two levels V^h and $V^{h/2}$ (left),and V^h and $V^{h/4}$ (right) for heat equation in 1D.

	$(u^h; \hat{z}^{h/2})$		$(u^h; \hat{z}^{h/4})$		
Nb of Elems	Est	Eff	Est	Eff	$Q_{e,e(T)}(e)$
16	3.6257e-04	0.7206	4.5308e-04	0.9005	5.0311e-04
32	9.0464e-05	0.7205	1.1307e-04	0.9006	1.2554e-04
64	2.2605e-05	0.7205	2.8255e-05	0.9007	3.1369e-05
128	5.6505e-06	0.7207	7.0631e-06	0.9009	7.8400e-06
256	1.4125e-06	0.7212	1.7657e-06	0.9015	1.9585e-06

Table 2: Estimate, error and effectivity for 100 time steps for heat equation in 1D.

$\hat{z}$ computed in spaces $V^{h/2}$ and $V^{h/4}$ with respect to uniform refinement. The effectivity index is ~ 0.7 when we use $\hat{z}^{h/2}$ to compute estimate, whereas it increases to ~ 0.9 with $\hat{z}^{h/4}$.

We observe that the additional cost of the computation is significant using the more expensive space $V^{h/4}$, however, the effectivity constants are still acceptable for the space $V^{h/2}$. Therefore, for the rest of the paper V^h and $V^{h/2}$ spaces will be used for the sake of computational cost.

2D Simulation Next, we ran the simulation in 2D with time step size of $\Delta t = 0.0005$ using the following initial condition

$$u(x, y, 0) = \sin(\pi x) \sin(\pi y).$$

In 2D, we compute the overkill solution using $2^8 \times 2^8$ elements and we use $2^2 \times 2^2, \ldots, 2^6 \times 2^6$ elements to compute $u^h \in V^h$. For the computation of the dual, we use the space $V^{h/2}$ with $2^3 \times 2^3, \ldots, 2^7 \times 2^7$ elements.

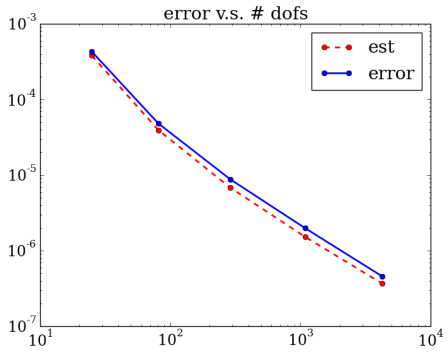

Figure 4: Convergence of error and estimate Est with respect to uniform refinement for single time step with two levels V^h and $V^{h/2}$ for heat equation in 2D.

	$(u^h; \hat{z}^{h/2})$		
Nb of Elems	Est	$Q_{e,e(T)}(e)$	Eff
4^2	3.8028e-04	4.2845e-04	0.8875
8^2	3.9390e-05	4.8174e-05	0.8176
16^2	6.806e-06	8.7837e-06	0.7748
32^2	1.5180e-06	1.9775e-06	0.7676
64^2	3.6813e-07	4.5946e-07	0.8012

Table 3: Estimate, error and effectivity for single time step for heat equation in 2D.

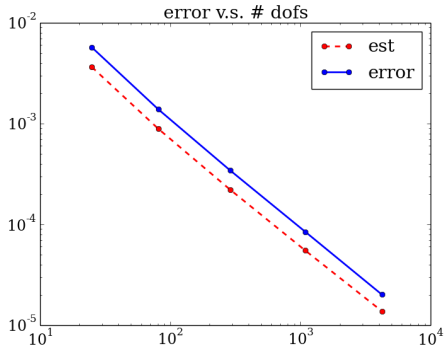

Figure 5: Convergence of error and estimate Est with respect to uniform refinement for 100 time steps with two levels V^h and $V^{h/2}$ for heat equation in 2D.

	$(u^h; \hat{z}^{h/2})$		
Nb of Elems	Est	$Q_{e,e(T)}(e)$	Eff
4^2	3.6420e-03	5.7110e-03	0.6377
8^2	8.8885e-04	1.3861e-03	0.6412
16^2	2.2091e-04	3.4304e-04	0.6439
32^2	5.5148e-05	8.4601e-05	0.6518
64^2	1.3782e-05	2.0134e-05	0.6845

Table 4: Estimate, error and effectivity for 100 time steps with two levels V^h and $V^{h/2}$ for heat equation in 2D.

In Figure 4 and 3, we present the convergence of estimate and the error with effectivity indices for one time step in 2D. The plot (left) shows that the estimate bounds the error asymptotically up to a constant which is presented in the table (right). Th effectivity index in ~ 0.8, which shows the estimate is effective.

We also consider the 2D test case, for 100 time steps, see Figure 5 and 4. We compute the estimate with $u^h \in V^h$ and $\hat{z}^{h/2} \in V^{h/2}$. One can see from the plot (left) that the estimate bounds the error up to a constant and the table (right) confirms that the constant

is ~ 0.6.

4.1.2 The Convective Cahn–Hilliard Equation

Next, the convective Cahn–Hilliard Equation is considered in mixed formulation, see Section 3.2.1. Since the Cahn–Hilliard equation is a nonlinear phase-field model, the estimation of errors can be illustrated with two test cases: Moving interface and merging two bubbles close to each other.

Similar to the heat equation approximation in Section 4.1.1, we define space-time primal and dual approximations with piecewise-constant reconstruction for the semi-implicit scheme applied to Galerkin finite element discretization of the mixed formulation. The reconstructions are:

$$u^h(t) = u^h_{k+1} \text{ and } \mu^h(t) = \mu^h_{k+1},\ t \in \big(t_k, t_{k+1}\big]$$

$$\hat{z}^{h/2}(t) = \hat{z}^{h/2}_{k+1} \text{ and } \hat{\chi}^{h/2}(t) = \hat{\chi}^{h/2}_{k+1},\ t \in \big[t_k, t_{k+1}\big)$$

for $k = 0, \ldots, N-1$. Then we can write estimate (42) as [3]

$$\begin{aligned} Est = \sum_{k=0}^{N-1} \Big\{ \Delta t \Big(&- (\mathbf{v}\nabla u^h_{k+1}, \hat{z}^{h/2}_k) - \frac{1}{Pe}(\nabla \mu^h_{k+1}, \nabla \hat{z}^{h/2}_k) - (\mu^h_{k+1}, \hat{\chi}^{h/2}_k) \\ &+ (\phi'(u^h_{k+1}), \hat{\chi}^{h/2}_k) + \varepsilon^2 (\nabla u^h_{k+1}, \nabla \hat{\chi}^{h/2}_k) \Big) - (u^h_{k+1} - u^h_k, \hat{z}^{h/2}_k) \Big\}. \end{aligned} \tag{47}$$

The discrete estimate (47) can be computed at each time step and summed up for the final time, T.

For the simulation of the Cahn–Hilliard equation, we choose $q_1 = \varepsilon^2 e^u$, $q_2 = e^\mu$ and $\bar{q} = e(T)$ as in (39) and we take $\varepsilon = 0.0625$ and $Pe = 1$.

Moving Interface We simulate the moving interface test case for 1D and 2D and we set the domain $\Omega = [0,1]^d$, for d$\in \{1, 2\}$. In 1D, we impose an initial condition for u_0 as:

$$u(x, 0) = \tanh\left(\frac{x - 0.25}{\sqrt{2}\varepsilon}\right),\ x \in [0, 1] \tag{48}$$

and we take $\mathbf{v} = 0.05$ for which the solution propagates as a front to the right.

[3] as in the heat equation case the piecewise-constant reconstruction can not be substituted immediately. The limiting procedure introduced in footnote 2 (page 20) also holds for the Cahn–Hilliard equation.

We compute Est with $u^h, \mu^h \in V^h$ and $\hat{z}^{h/2}, \hat{\chi}^{h/2} \in V^{h/2}$, for which we use $2^3, \ldots, 2^9$ and $2^4, \ldots, 2^{10}$ elements, respectively. For the overkill solution, we use 2^{13} elements. In order to obtain higher effectivity, we also choose two times refined space than V^h, which is $V^{h/4}$ with $2^5, \ldots, 2^{11}$ elements.

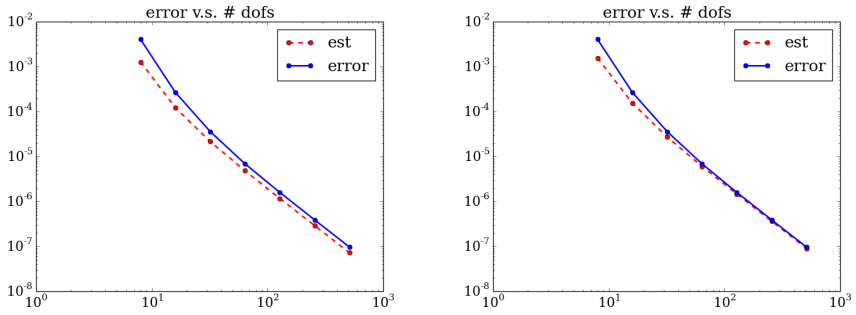

Figure 6: Convergence of error and estimate Est with respect to uniform refinement for 100 time steps with two levels V^h and $V^{h/2}$ (left), and V^h and $V^{h/4}$ (right) for Cahn–Hilliard equation, moving interface test case in 1D.

	$(u^h, \mu^h; \hat{z}^{h/2}, \hat{\chi}^{h/2})$		$(u^h, \mu^h; \hat{z}^{h/4}, \hat{\chi}^{h/4})$		
Nb of Elems	Est	Eff	Est	Eff	$Q_{e^u, e^\mu, e^u(T)}(e)$
16	1.2205e-04	0.4559	1.5419e-04	0.5760	2.6772e-04
32	2.1533e-05	0.6002	2.7088e-05	0.7550	3.5876e-05
64	4.8082e-06	0.6987	6.0224e-06	0.8751	6.8813e-06
128	1.1656e-06	0.7350	1.4578e-06	0.9193	1.5857e-06
256	2.8913e-07	0.7457	3.6146e-07	0.9323	3.8771e-07

Table 5: Effectivity of 100 time steps estimate for Cahn–Hilliard equation, moving interface test case in 1D.

We present the convergence plots in Figure 6 for 100 time steps in 1D with $\Delta t = 0.0005$. One can observe that the estimate bounds the error asymptotically up to a constant for both plots. The estimate gets closer to the error when $(\hat{z}^{h/4}, \hat{\chi}^{h/4})$ is used instead of $(\hat{z}^{h/2}, \hat{\chi}^{h/2})$.

Similarly, Table 5 enables a fair comparison of error, estimate and effectivity. Effectivity index increases, if the computation is done using the pair $(\hat{z}^{h/4}, \hat{\chi}^{h/4})$ instead of $(\hat{z}^{h/2}, \hat{\chi}^{h/2})$.

We also ran the simulation in 2D and use the initial condition

$$u(x, y, 0) = \tanh\left(\frac{x - 0.25}{\sqrt{2}\varepsilon}\right), \ (x, y) \in [0, 1] \times [0, 1] \tag{49}$$

with $\mathbf{v} = (0.05, 0)$. $u^h, \mu^h \in V^h$ are computed with $2^2 \times 2^2, \ldots, 2^6 \times 2^6$ elements and for the dual pair $\hat{z}^{h/2}, \hat{\chi}^{h/2} \in V^{h/2}$ we use $2^3 \times 2^3, \ldots, 2^7 \times 2^7$ elements. The overkill solution is computed with $2^8 \times 2^8$ elements.

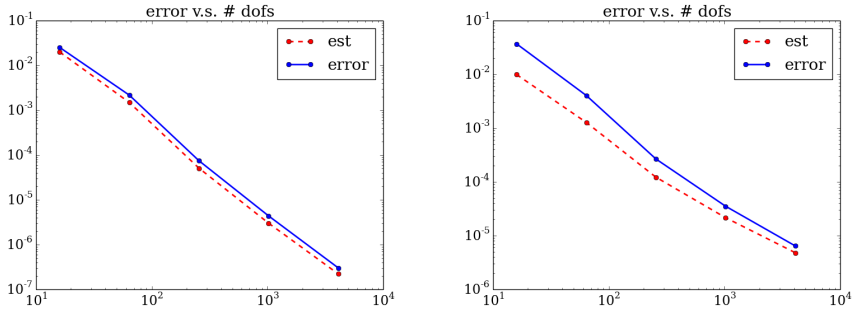

Figure 7: Convergence of errror and estimate Est with respect to uniform refinement for 1 (left) and 100 (right) time steps with two levels V^h and $V^{h/2}$ for Cahn–Hilliard equation, moving interface test case in 2D.

	$T = 0.0005$			$T = 0.05$		
Nb of Elems	Est	$Q_{e^u,e^\mu,e^u(T)}(e)$	Eff	Est	$Q_{e^u,e^\mu,e^u(T)}(e)$	Eff
4^2	1.9926e-02	2.5232e-02	0.7897	9.9011e-03	3.6916e-02	0.2682
8^2	1.4882e-03	2.1692e-03	0.6860	1.2766e-03	4.0469e-03	0.3154
16^2	5.0831e-05	7.4457e-05	0.6827	1.2204e-04	2.6622e-04	0.4584
32^2	3.0019e-06	4.3608e-06	0.6883	2.1531e-05	3.5200e-05	0.6116
64^2	2.2099e-07	3.0101e-07	0.7342	4.8088e-06	6.4280e-06	0.7481

Table 6: Effectivity of 1 and 100 time steps estimate for Cahn–Hilliard equation, moving interface test case in 2D.

In Figure 7 and Table 6, 1 and 100 time steps results are considered. In both of the plots of Figure 7 we observe the convergence behavior such that the error is bounded below asymptotically. In the pre-asymptotics, we can see from left plot of Figure 7 that the error and the estimate are converging with the same order for 1 time step. For 100 time step, they start with a low convergence rate, then estimate gets closer to the error as the number of dofs increase. This is also confirmed by the effectivity indices in Table 6.

Remark 4.2 We also test the two-level estimator based on a linear quantity of interest:

$$Q(u) := \int_\Omega \sin(\pi x) u(T)\, d\Omega, \tag{50}$$

□

which is obtained by choosing $q = 0$ and $\bar{q} = \sin(\pi x)$ in (5), for which the estimate is again of the same form as in (47).

The results presented in Figure 8 and Table 7 are obtained for the moving interface test case of 1D Cahn–Hilliard equation for 100 time steps with $\Delta t = 0.00001$ under uniform refinement, and confirm the expected consistency of the estimator. The convergence behavior slightly deviates because of errors due to time discretization (not taken into account).

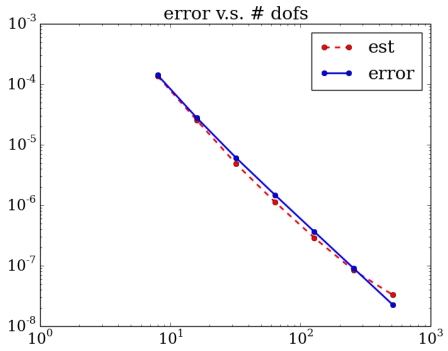

Figure 8: Convergence of error and estimate *Est* with respect to uniform refinement for 100 time steps with two levels V^h and $V^{h/2}$ for Cahn–Hilliard equation, moving interface test case in 1D and for $Q(\cdot)$ in (50).

	$(u^h, \mu^h; \hat{z}^{h/2}, \hat{\chi}^{h/2})$		
Nb of Elems	Est	$Q_{e,1}(e)$	Eff
16	2.5443e-05	2.7887e-05	0.9123
32	4.8486e-06	6.1084e-06	0.7937
64	1.1236e-06	1.4727e-06	0.7629
128	2.8921e-07	3.6475e-07	0.7929
256	8.4079e-08	9.0913e-08	0.9248

Table 7: Estimate error and effectivity for 100 time steps with two levels V^h and $V^{h/2}$ for Cahn–Hilliard equation, moving interface test case in 1D and for $Q(\cdot)$ in (50).

Merging Bubble in 2D The final numerical experiment is the case of two bubbles merging. We consider the error measure of (36) by aiming to estimate the error particularly for the physics of a topological change. We take the Cahn–Hilliard equation without convection, i.e., $\mathbf{v} = 0$ and take the following initial condition corresponding to kissing bubbles of the same radius, 0.2 in $\Omega = [0, 1] \times [0, 1]$:

$$u(x, 0) = 1 + \tanh\left(\frac{0.2 - \sqrt{(x - 0.25)^2 + y^2}}{\sqrt{2}\varepsilon}\right) + \tanh\left(\frac{0.2 - \sqrt{(x + 0.25)^2 + y^2}}{\sqrt{2}\varepsilon}\right).$$

We present 2D results with time step size, $\Delta t = 0.0005$ for 200 time steps. In Figure 9, the solution of the merging case can be seen.

In this test case, the effectivity is low for small number of elements, see Figure 10 and 11. However, the effectivity increases up to 0.4145, once the mesh captures the interface. For this last case, the effectivity would increase if we increase the number of refinements.

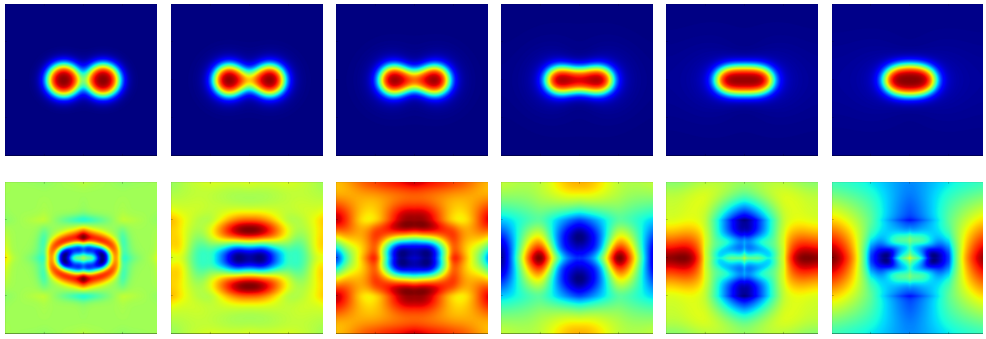

Figure 9: Two merging bubbles in 2D: primal, u (top), dual χ (bottom)

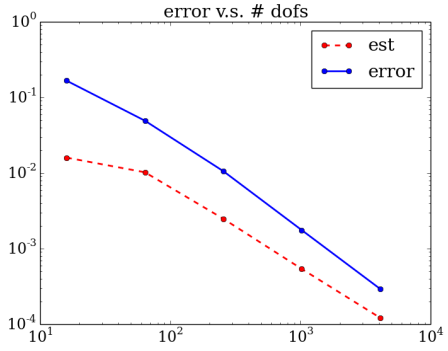

Figure 10: Convergence of error and estimate *Est* with respect to uniform refinement for 200 time steps with two levels V^h and $V^{h/2}$ for Cahn–Hilliard equation, merging bubble test case in 2D.

	$(u^h, \mu^h; \hat{z}^{h/2}, \hat{\chi}^{h/2})$		
Nb of Elems	Est	$Q_{e,e(T)}(e)$	Eff
4^2	1.5969e-02	1.6640e-01	0.0959
8^2	1.0217e-02	4.9134e-02	0.2079
16^2	2.4790e-03	1.0568e-03	0.2345
32^2	5.3838e-04	1.7559e-03	0.3066
64^2	1.2160e-04	2.9331e-4	0.4145

Figure 11: Estimate, error and effectivity for 200 time steps with two levels V^h and $V^{h/2}$ for Cahn–Hilliard equation, merging bubble test case in 2D.

Remark 4.3 (Direct error estimation) For a merging bubble test case in 1D, Figure 12 shows a comparison of time-contributions to the two-level estimator (blue curve) and the *direct* space-time error estimator $||u^{h/2} - u^h||^2 := \int_0^T \left(\varepsilon^2 \|\nabla\left(u^{h/2} - u^h\right)\|^2 + \frac{1}{Pe}\|\nabla\left(\mu^{h/2} - \mu^h\right)\|^2\right) dt$ (red curve). As explained in the introduction, the two-level estimator contributions indicate the sensitivity of the quantity of interest to errors accumulated at earlier times. In Figure 12, the blue curve indicates that this is mostly for the time interval that merging happens, that is, for t between 0.10 and 0.15. On the other hand, the direct-estimator contributions do not necessarily point to sensitivity of the quantity of interest. Indeed, the red curve has significant contributions throughout the time interval, and in particular at the beginning.

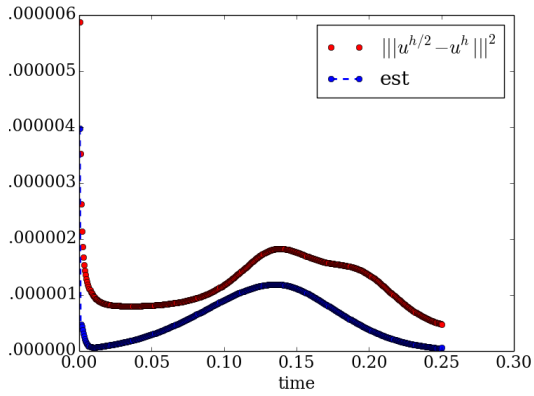

Figure 12: Comparison of time-contributions to Est and $\|u^{h/2} - u^h\|^2$.

4.2 Adaptivity

We now consider adaptivity based on the indicators, which contain not only the information for the current time step but also the whole evolution history implicitly via the dual. The proposed global-time space-adaptive algorithm for our error measure (8) is presented in Algorithm 1.

The numerical test cases we provide later are preliminary adaptive tests aimed at demonstrating how the new estimator can be employed in the adaptive strategy. And for the sake of simplification, we only consider adaptivity in space.

We note that adaptivity for time-dependent problems has additional overhead in its numerical implementation, such as projection / interpolation between meshes, and multiple space-time solves. However, the advantage of adaptivity is clear: one obtains optimized meshes at each time instance for the solution at hand.

The computable estimator (14) is a global space-time residual weighted with the dual approximation. Assuming piecewise-constant reconstruction of the primal solution and the dual solution, the estimator splits up as,

$$Est = \sum_{k=0}^{N-1} \left(\Delta t \, \mathcal{R}^t(u_{k+1}^h; \hat{z}_k^{h/2}) + (u_k^h - u_{k+1}^h, \hat{z}_k^{h/2}) \right) \leq \sum_{k=0}^{N-1} Est_k \tag{51}$$

where

$$Est_k := \left| \Delta t \, \mathcal{R}^t(u_{k+1}^h; \hat{z}_k^{h/2}) + (u_k^h - u_{k+1}^h, \hat{z}_k^{h/2}) \right|. \tag{52}$$

We may thus localize the estimator to indicate the space error contributions at each time step k. To further localize the estimator in space, we use the decomposition into shape

Algorithm 1 The global-time space-adaptive algorithm

Choose an initial coarse mesh $\mathcal{K}$ and a small enough time step size Δt
Initialize a list of mesh $\{\mathcal{K}_1, ..., \mathcal{K}_N\}$, one individual mesh for one time step
while the maximal error estimate $MAX >$ tolerance **do**
  for every time step k $(t := 0 \to T)$ **do**
    Compute the primal solution u_k^h using the current mesh $\mathcal{K}_k$
    Compute the primal solution $u_k^{h/2}$ using the finer mesh $\mathcal{K}_k^{h/2}$(i.e. $\mathcal{K}_k^{h/2}$ is the uniform refinement of $\mathcal{K}_k$)
  end for
  for every time step k $(t := T \to 0)$ **do**
    Compute the dual solution $\hat{z}_k^{h/2}$ using the finer mesh $\mathcal{K}_k^{h/2}$
    Estimate the current mesh error contribution Est_k
  end for
  Compute the maximal error contribution for the whole time period $MAX = \max\{Est_1, ..., Est_N\}$
  while $|Est_k| > \theta\,|MAX|$ **do**
    Estimate the local error contribution η_k^i for the mesh $\mathcal{K}_k$
    Refine the mesh $\mathcal{K}_k$ by using hierarchical refinement strategy and maximum strategy with parameter λ
  end while
end while

functions $\varphi^i \in V^{h/2}$, $i = 1, ..., M$. The dual solution can be written as the linear combination,

$$\hat{z}_k^{h/2} = \sum_{i=1}^{M} \tilde{z}_k^i \varphi^i. \tag{53}$$

Inserting the ansatz (53) into (52), we get

$$Est = \sum_{k=0}^{N-1} \sum_{i=1}^{M} \Big(\Delta t \ \tilde{z}_k^i \ \mathcal{R}^t(u_{k+1}^h; \varphi^i) + \tilde{z}_k^i \ (u_k^h - u_{k+1}^h, \varphi^i) \Big). \tag{54}$$

Thus, the error estimator is localized to the basis. This is similar to the localization approach in [10]. The indicator for each basis function φ^i in $V^{h/2}$ at each time step k is thus:

$$\eta_k^i = \Delta t \ \tilde{z}_k^i \ \mathcal{R}^t(u_{k+1}^h; \varphi^i) + \tilde{z}_k^i \ \left(u_k^h - u_{k+1}^h, \varphi^i \right). \tag{55}$$

The same as localizing the indicator, the error control is also built on a two-step approach. First, we apply the maximum marking strategy with fraction $\theta \in [0, 1]$ on Est_k, to select which time steps contain the big error contributions throughout the time period. To reduce the error, the corresponding space meshes at the selected time steps are targeted to be refined. Then, the maximum marking strategy is applied second time for selecting basis function in $V^{h/2}$. The indicator of the selected basis is at least a fraction $\lambda \in [0, 1]$ bigger than the maximal indicator (i.e. $|\eta_i| \geq \lambda \max(|\eta_i|)$).

The mesh refinement is based on the hierarchical refinement strategy in [45, 26]. Since $V^{h/2}$ is the uniform refined space of V^h, the parents of the basis functions in $V^{h/2}$ are the basis functions in V^h. Thus, for the selected basis in $V^{h/2}$, the mesh in V^h can be refined according to the parent of the basis in $V^{h/2}$.

Remark 4.4 (Hierarchical Indicator) In general, the standard indicator for the dual weighted residual (DWR) method is obtained by applying integration by parts after localizing the indicator elementwise as in [6]. In particular, for the DWR indicators, the interpolant of the dual solution, $I\hat{z}_k^{h/2}$, is subtracted from $\hat{z}_k^{h/2}$ to get a sharper indicator. However, for hierarchical indicators, like (55), instead of using integration by parts, the indicator is localized through patches of elements corresponding to the support of basis functions. Hence, the indicator in (55) is expected to be sharp. Let us show that (55) is equivalent to the indicator obtained by localizing the residual weighted by $\hat{z}_k^{h/2} - I\hat{z}_k^{h/2}$. Consider

$$\eta_k = \Delta t \ \mathcal{R}^t \left(u_{k+1}^h; (\hat{z}_k^{h/2} - I\hat{z}_k^{h/2}) \right) + \left(u_k^h - u_{k+1}^h, (\hat{z}_k^{h/2} - I\hat{z}_k^{h/2}) \right), \tag{56}$$

where, by Galerkin orthogonality,

$$\Delta t\ \mathcal{R}^t\left(u_{k+1}^h; I\hat{z}_k^{h/2}\right) + \left(u_k^h - u_{k+1}^h, I\hat{z}_k^{h/2}\right) = 0.$$

The interpolant $I\hat{z}_k^{h/2}$, similar to (53), can be written as a linear combination of shape functions:

$$I\hat{z}_k^{h/2} = \sum_{i=1}^{M} \bar{z}_k^i \varphi^i = \sum_{i=1}^{M} \tilde{z}_k^i I\varphi^i,$$

then (56) can be rewritten as

$$\begin{aligned}
\eta_k &= \sum_{i=1}^{M} \left(\Delta t\ \mathcal{R}^t(u_{k+1}^h; \tilde{z}_k^i\varphi^i - \bar{z}_k^i\varphi^i) + (u_k^h - u_{k+1}^h, \tilde{z}_k^i\varphi^i - \bar{z}_k^i\varphi^i)\right) \\
&= \sum_{i=1}^{M} \left(\Delta t\ \mathcal{R}^t(u_{k+1}^h; \tilde{z}_k^i\varphi^i - \tilde{z}_k^i\ I\varphi^i) + (u_k^h - u_{k+1}^h, \tilde{z}_k^i\varphi^i - \tilde{z}_k^i\ I\varphi^i)\right). \\
&= \sum_{i=1}^{M} \left(\Delta t\ \tilde{z}_k^i\ \mathcal{R}^t\left(u_{k+1}^h; \left(\varphi^i - \ I\varphi^i\right)\right) + \tilde{z}_k^i\ \left(u_k^h - u_{k+1}^h, \left(\varphi^i - \ I\varphi^i\right)\right)\right).
\end{aligned}$$

Hence, Galerkin orthogonality

$$\Delta t\ \mathcal{R}^t\left(u_{k+1}^h; I\varphi^i\right) + \left(u_k^h - u_{k+1}^h, I\varphi^i\right) = 0$$

implies

$$\begin{aligned}
\eta_k^i &= \Delta t\ \tilde{z}_k^i\ \mathcal{R}^t(u_{k+1}^h; \varphi^i) + \tilde{z}_k^i\ \left(u_k^h - u_{k+1}^h, \varphi^i\right) \\
&= \Delta t\ \tilde{z}_k^i\ \mathcal{R}^t(u_{k+1}^h; \left(\varphi^i - \ I\varphi^i\right)) + \tilde{z}_k^i\ \left(u_k^h - u_{k+1}^h, \left(\varphi^i - \ I\varphi^i\right)\right)
\end{aligned}$$

which coincides with the localized indicator (55). □

4.2.1 Heat Equation

We begin with verifying numerically our global-time space-adaptive algorithm with the linear heat equation (21). The dynamics of this test case is one bubble smoothed out in the middle of the domain. The initial condition is assumed to be:

$$u(x,0) = \tanh\left(50\left(0.2 - \sqrt{x^2+y^2}\right)\right) + 1 \tag{57}$$

We take the time step size $\Delta t = 0.0005$, the final time $T = 0.025$, the initial coarse mesh with 8^2 elements in the domain $\Omega = [-1,1]^2$, and the adaptive setting $\theta = 0.8$, $\lambda = 0.7$.

Figure 13 shows the change of the estimator Est_k after different refinements. In the first plot, we can see that the largest error contribution is from the first time step. Thus, the algorithm selects the mesh of the first time step. The second plot shows that the peak error at the first time step has indeed decreased. And the peak has now shifted to another time step. In the end, all the error contribution at every time step is under our tolerance.

The comparison between the final refinement result and the exact solution is presented in Figure 14. Let us mention that, for better visualization, in the plots the colors represent different values for each plot in time. In the first column of plots $t = 0.0005$, the color scale of the exact solution and the adaptive solution are both from 0.0 to 2.0. Then, both solutions are smoothed out by the nature of heat equation. In the last column of plots $t = 0.025$, the color scale of both solutions are from 0.0 to 0.64. The first row of the figure shows snapshots of the solution at a fine uniform mesh which is composed of 256×256 elements. We treat this solution as the exact solution. The second row show the time-history of the numerical solution using the adaptive algorithm.

4.2.2 The Cahn-Hiliard Equation

In this test case, we consider the dynamics of two bubbles merging. The initial condition of the Cahn-Hilliard Equation without convective term is

$$u(x,0) = \tanh\left(\frac{0.2 - \sqrt{(x-0.3)^2 + y^2}}{\sqrt{2}\varepsilon}\right) + \tanh\left(\frac{0.2 - \sqrt{(x+0.3)^2 + y^2}}{\sqrt{2}\varepsilon}\right) + 1 \quad (58)$$

where $\epsilon = 0.0625$, $Pe = 1$, $\Omega = [-1,1]^2$. The fractions in the maximum strategies are $\theta = 0.8$ and $\lambda = 0.8$. The time step size $\Delta t = 0.0005$, and the final time $T = 0.015$. The initial coarse mesh and the adaptive setting is the same as heat equation. Figure 15 shows the change of the estimator in time after different refinements. The result of two bubbles merging is shown in Figure 16. The exact solution is computed by using the uniform mesh composed of 256×256 elements. In the plots the colors represent the same values from -1 to 1. According to Figure 15 and Figure 16, the estimator has high value at the beginning and the end. Thus, the corresponding mesh is driven by the estimator, to have finer mesh at first time step and in the end.

5 Conclusion

In this paper, we introduced a duality-based two-level a posteriori error estimate in a general framework for nonlinear time-dependent PDEs. We employed linearization and

computed the estimate with primal and dual problems approximated in two different discrete spaces. We also presented a consistency theorem which shows that the error is equal to sum of the estimate and remainders with all possible sources of errors: linearization, primal approximation and dual discretization. We tested our estimate for heat and Cahn–Hilliard equations for one and multiple time steps and for various mesh sizes. Numerical experiments verified the effectivity of the estimate and gave more accurate results when we use a better second level discrete space. Furthermore, we presented space adaptivity results for both of the equations using a global space-time adaptive algorithm. Adaptivity addressed the meshes where critical changes happen according to our error measure in space-time norm.

In the future, we intend to carry out a comprehensive study of various adaptive strategies based on the developed duality-based two-level estimate for more complicated cases such as topological changes and compare it to other adaptive strategies.

Acknowledgements

The support of this work by the Netherlands Organisation for Scientific Research (NWO) via the Innovational Research Incentives Scheme (IRIS), Veni grant 639.031.033 and by NanoNextNL, a micro and nanotechnology consortium of the Government of the Netherlands and 130 partners, is gratefully acknowledged. The authors would like to express their thanks to Gertjan van Zwieten for his help related to numerical implementations in the Nutils software (Nutils.org).

References

[1] H. Abels, H. Garcke, and G. Grün, *Thermodynamically consistent, frame indifferent diffuse interface models for incompressible two-phase flows with different densities*, Math. Models Methods Appl. Sci., 22 (2012), pp. 1150013–1–40.

[2] M. Ainsworth and J. T. Oden, *A Posteriori Error Estimation In Finite Element Analysis*, Pure Appl. Math., Wiley, 2000.

[3] W. Bangerth and R. Rannacher, *Adaptive Finite Element Methods for Differential Equations*, Lectures in Mathematics, ETH Zürich, Birkhäuser, 2003.

[4] R. E. Bank, *Hierarchical bases and the finite element method.*, Acta Numerica, (1996).

[5] S. Bartels and R. Müller, *A posteriori error controlled local resolution of evolving interfaces for generalized Cahn–Hilliard equations*, Interfaces Free Bound., 12 (2010), pp. 45–73.

[6] R. Becker and R. Rannacher, *An optimal control approach to a posteriori error estimation in finite element methods*, Acta Numer., 10 (2001), pp. 1–102.

[7] M. J. Borden, C. V. Verhoosel, M. A. Scott, T. J. R. Hughes, and C. M. Landis, *A phase-field description of dynamic brittle fracture*, Comput. Methods Appl. Mech. Engrg., 217-220 (2012), pp. 77 – 95.

[8] B. Bourdin, G. A. Francfort, and J.-J. Marigo, *The variational approach to fracture*, 91 (2008), pp. 5–148.

[9] M. Braack, E. Burman, and N. Taschenberger, *Duality based a posteriori error estimation for quasi-periodic solutions using time averages*, SIAM J. Sci. Comput., 33 (2011), pp. 2199–2216.

[10] M. Braack and A. Ern, *A posteriori control of modeling errors and discretization errors*, Multiscale Model. Simul., 1 (2003), pp. 221–238.

[11] V. Carey, D. Estep, A. Johansson, M. Larson, and S. Taverner, *Blockwise adaptivity for time dependent problems based on coarse scale adjoint solutions*, SIAM J. Sci. Comput., 32 (2010), pp. 2121–2145.

[12] V. Dolejši, A. Ern, and M. Vohralík, *A framework for robust a posteriori error control in unsteady nonlinear advection-diffusion problems*, SIAM J. Numer. Anal., 51 (2013), pp. 773–793.

[13] K. Eriksson, D. Estep, P. Hansbo, and C. Johnson, *Introduction to adaptive methods for differential equations*, Acta Numer., (1995), pp. 1–54.

[14] K. Eriksson, C. Johnson, and A. Logg, *Adaptive computational methods for parabolic problems*, in Encyclopedia of Computational Mechanics, E. Stein, R. de Borst, and T. J. R. Hughes, eds., vol. 1: Fundamentals, John Wiley & Sons, 2004, ch. 24, pp. 675–702.

[15] A. Ern and J.-L. Guermond, *Theory and Practice of Finite Element Methods*, vol. 159 of Applied Mathematical Sciences, Springer-Verlag, New York, 2004.

[16] D. Estep, M. Holst, and D. Mikulencak, *Accounting for stability: a posteriori error estimates based on residuals and variational analysis*, Comm. Numer. Meth. Engrg., 18 (2002), pp. 15–30.

[17] L. C. Evans, *Partial Differential Equations*, vol. 19 of Graduate Studies in Mathematics, American Mathematical Society, Providence, Rhode Island, 1998.

[18] D. Eyre, *An unconditionally stable one-step scheme for gradient systems*, tech. rep., Department of Mathematics, University of Utah, Salt Lake City, Utah, USA, 1997. unpublished.

[19] M. B. Giles and E. Süli, *Adjoint methods for PDEs: A posteriori error analysis and postprocessing by duality*, Acta Numer., (2002), pp. 145–236.

[20] H. Gomez and T. J. R. Hughes, *Provably unconditionally stable, second-order time-accurate, mixed variational methods for phase-field models*, J. Comput. Phys., 230 (2011), pp. 5310–5327.

[21] A. Hawkins-Daarud, K. G. van der Zee, and J. T. Oden, *Numerical simulation of a thermodynamically consistent four-species tumor growth model*, Int. J. Numer. Meth. Biomed. Engng., 28 (2011), pp. 3–24.

[22] J. Hoffman and C. Johnson, *Stability of the dual Navier–Stokes equations and efficient computation of mean output in turbulent flow using adaptive DNS/LES*, Comput. Methods Appl. Mech. Engrg., 195 (2006), pp. 1709–1721.

[23] M. Holst, J. S. Ovall, and R. Szypowski, *An efficient, reliable and robust error estimator for elliptic problems in* $\mathbb{R}^3$, Appl. Numer. Math., 61 (2011), pp. 675–695.

[24] D. Kessler, R. H. Nochetto, and A. Schmidt, *A posteriori error control for the Allen–Cahn problem: Circumventing Gronwall's inequality*, M2AN Math. Model. Numer. Anal., 38 (2004), pp. 129–142.

[25] J. Kim and J. Lowengrub, *Phase field modeling and simulation of three-phase flows*, Interfaces Free Bound., 7 (2005), pp. 435–466.

[26] G. Kuru, *Goal-adaptive isogeometric analysis with hierarchical splines*, Master's thesis, Multiscale Engineering Fluid Dynamics, Eindhoven University of Technology, Eindhoven, Netherlands, 2013.

[27] F. Larsson, P. Hansbo, and K. Runesson, *Strategies for computing goal-oriented a posteriori error measures in non-linear elasticity*, Int. J. Numer. Meth. Engng., 55 (2002), pp. 879–894.

[28] C. Makidakis and R. H. Nochetto, *Elliptic reconstruction and a posteriori error estimates for parabolic problems*, SIAM J. Numer. Anal., pp. 1585–1594.

[29] R. H. Nochetto, A. Schmidt, and C. Verdi, *A posteriori error estimation and adaptivity for degenerate parabolic problems*, Math. Comp., 69 (2000), pp. 1–24.

[30] J. T. Oden, A. Hawkins, and S. Prudhomme, *General diffuse-interface theories and an approach to predictive tumor growth modeling*, Math. Models Methods Appl. Sci., 20 (2010), pp. 477–517.

[31] J. T. Oden and S. Prudhomme, *Goal-oriented error estimation and adaptivity for the finite element method*, Comput. Math. Appl., 41 (2001), pp. 735–756.

[32] J. S. Ovall, *Asymptotically exact functional error estimators based on superconvergent gradient recovery*, Numer. Math., 102 (2006), pp. 543–558.

[33] N. Parés, P. Díez, and A. Huerta, *Bounds of functional outputs for parabolic problems. Part I: Exact bounds of the discontinuous Galerkin time discretization*, Comput. Methods Appl. Mech. Engrg., 197 (2008), pp. 1641–1660.

[34] ——, *Bounds of functional outputs for parabolic problems. Part II: Bounds of the exact solution*, Comput. Methods Appl. Mech. Engrg., 197 (2008), pp. 1661–1679.

[35] S. Perotto and A. Veneziani, *Coupled model and grid adaptivity in hierarchical reduction of elliptic problems*, J. Sci. Comput., (2013), pp. 1–32.

[36] N. Provatas and K. Elder, *Phase-Field Methods in Materials Science and Engineering*, Wiley-VCH, Weinheim, 2010.

[37] R. H. Stogner, G. F. Carey, and B. T. Murray, *Approximation of Cahn–Hilliard diffuse interface models using parallel adaptive mesh renement and coarsening with C^1 elements*, Int. J. Numer. Meth. Engng., 76 (2008), pp. 636–661.

[38] K. G. van der Zee, *Goal-Adaptive Discretization of Fluid–Structure Interaction*, PhD thesis, Technische Universiteit Delft, Delft, The Netherlands, June 2009.

[39] K. G. van der Zee, J. T. Oden, S. Prudhomme, and A. Hawkins-Daarud, *Goal-oriented error estimation for Cahn–Hilliard models of binary phase transition*, Numer. Methods Partial Differential Equations, 27 (2011), pp. 160–196.

[40] K. G. van der Zee, E. H. van Brummelen, I. Akkerman, and R. de Borst, *Goal-oriented error estimation and adaptivity for fluid–structure interaction using exact linearized adjoints*, Comput. Methods Appl. Mech. Engrg., 200 (2011), pp. 2738–2757.

[41] K. G. van der Zee, E. H. van Brummelen, and R. de Borst, *Goal-oriented error estimation and adaptivity for free-boundary problems: The domain-map linearization approach*, SIAM J. Sci. Comput., 32 (2010), pp. 1064–1092.

[42] F. Verdugo, N. Parés, and P. Díez, *Error assessment in stuctural transient dynamics*, Arch. Comput. Methods Eng., 21 (2014), pp. 59–90.

[43] R. Verfürth, *A Review of A Posteriori Error Estimation and Adaptive Mesh-Refinement Techniques*, Advances in Numerical Mathematics, Wiley-Teubner, New York, Stuttgart, 1996.

[44] ——, *A posteriori error estimates for nonlinear problems: $l^r(0,t;w^1 1,\rho(\omega)$-error estimates for finite element discretizations of parabolic equations*, Math. Comp., 67 (1998), pp. 1335–1360.

[45] A.-V. Vuong, C. Giannelli, B. Jüttler, and B. Simeon, *A hierarchical approach to adaptive local refinement in isogeometric analysis*, Comput. Methods Appl. Mech. Engrg., 200 (2011), pp. 3554–3567.

[46] X. Wu, G. J. van Zwieten, and K. G. van der Zee, *Stabilized second-order splitting schemes for Cahn–Hilliard models with application to diffuse-interface tumor-growth models*, Int. J. Numer. Meth. Biomed. Engng., 30 (2014), pp. 180–203.

[47] C. W. Z. Guan, J. S. Lowengrub and S. M. Wise, *Second order convex splitting schemes for periodic nonlocal cahn–hilliard and allen–cahn equations.* preprint, 2013.

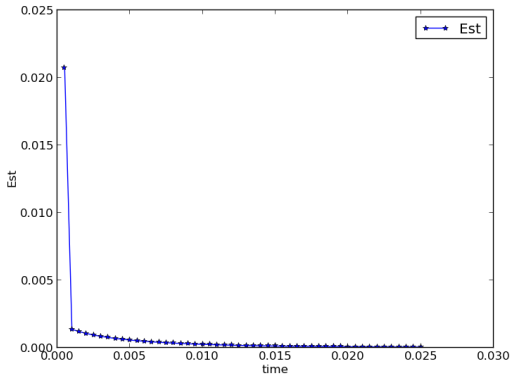

$refinement = 0$

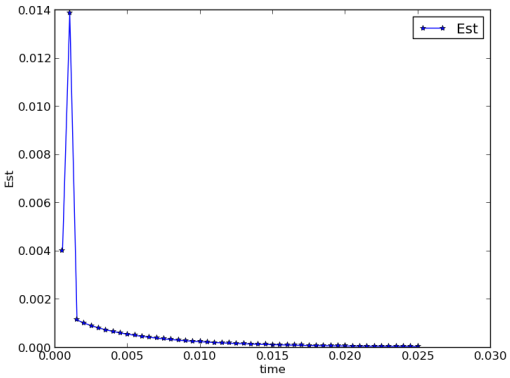

$refinement = 1$

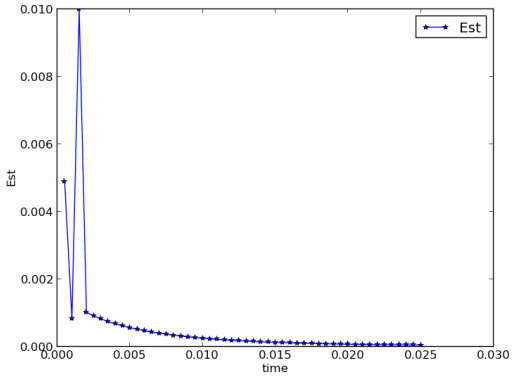

$refinement = 2$

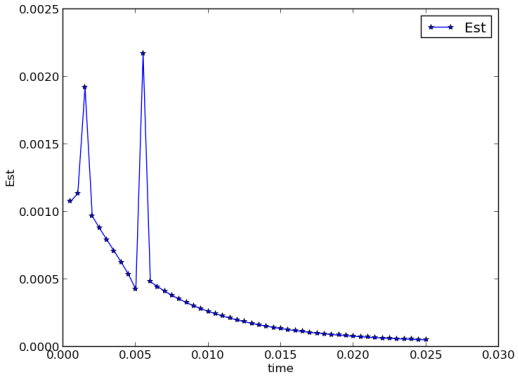

$refinement = 10$

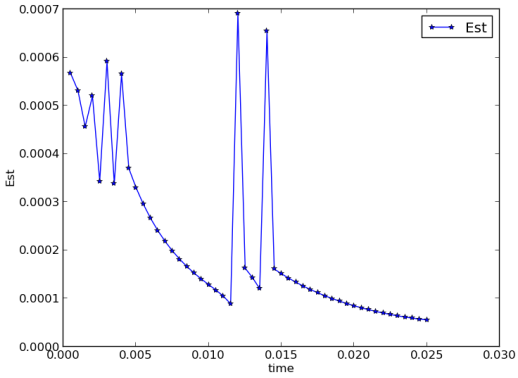

$refinement = 30$

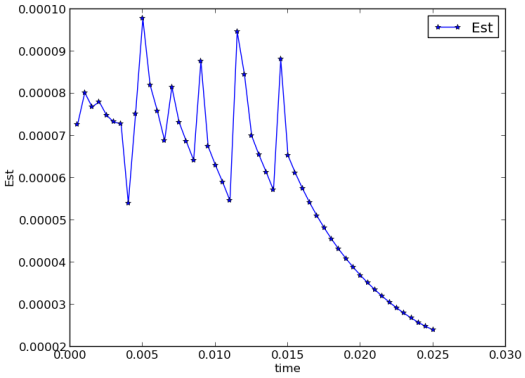

$refinement = 60$

Figure 13: Global space estimator Est_k versus time

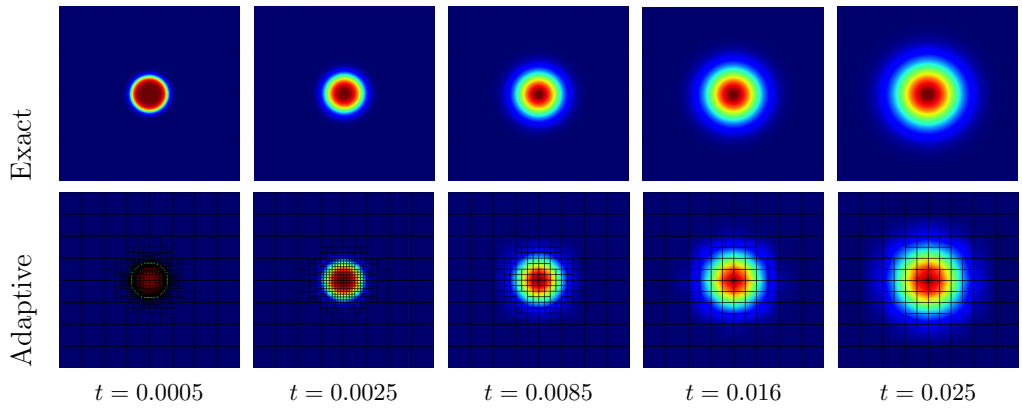

Figure 14: One bubble smoothing in 2D

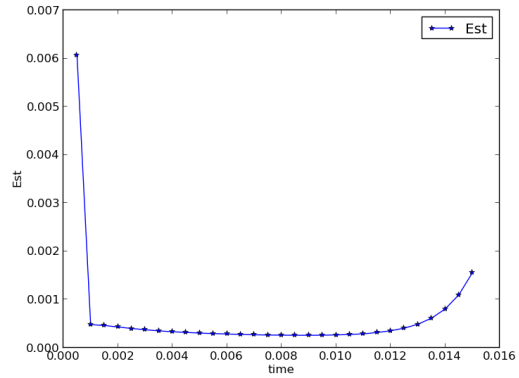

$refinement = 0$

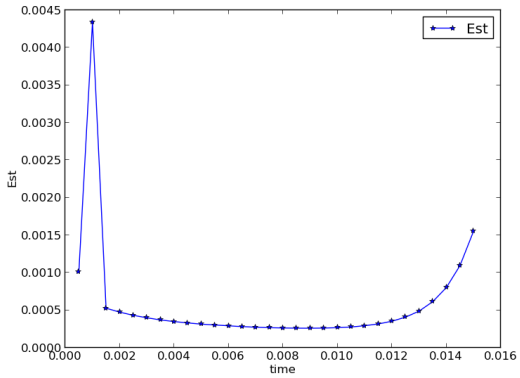

$refinement = 1$

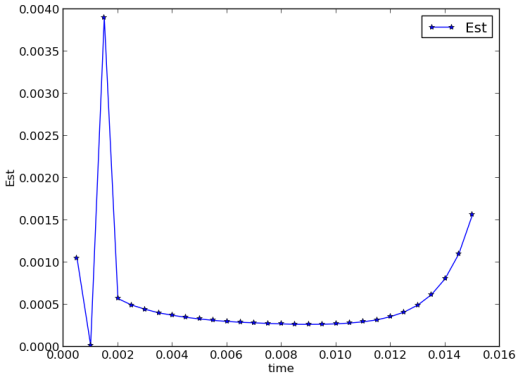

$refinement = 2$

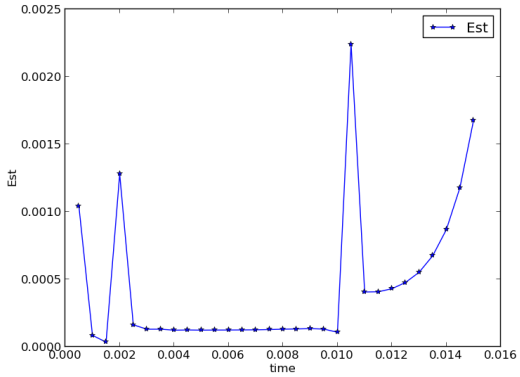

$refinement = 20$

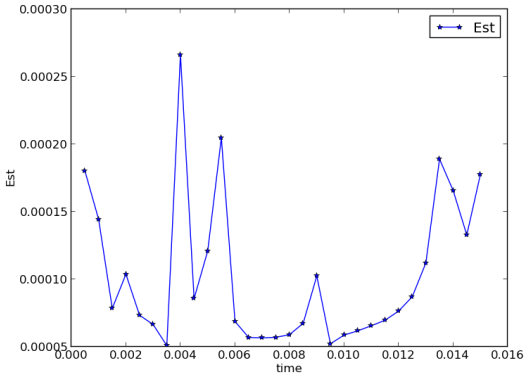

$refinement = 70$

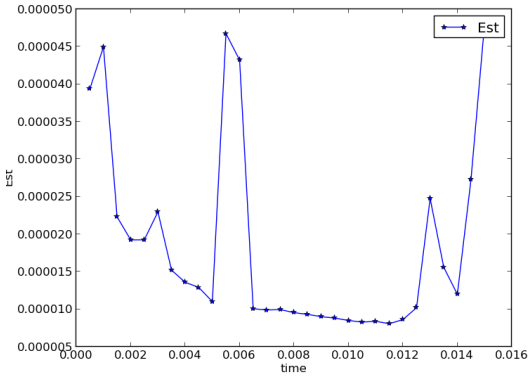

$refinement = 130$

Figure 15: Global space estimator Est_k versus time

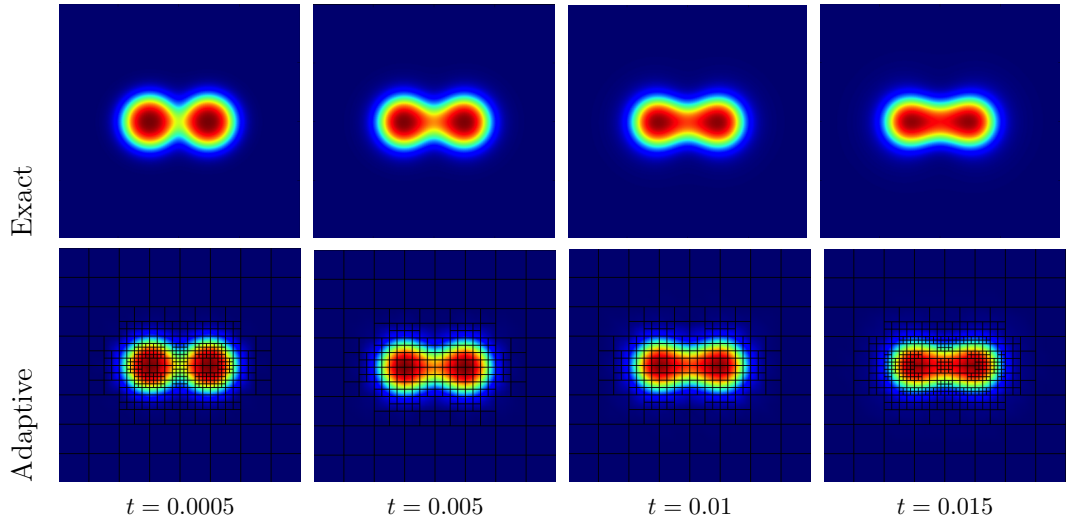

Figure 16: Two bubble merging in 2D